FFI RAPPORT

Mechanical studies of wolfram carbide

Frøyland Øyvind, Moxnes John F

FFI/RAPPORT-2004/03860

FFI-V/860/01

Approved
Kjeller 2004-11-10

Bjarne Haugstad
Director of Research

Mechanical studies of wolfram carbide

Frøyland Øyvind, Moxnes John F

FFI/RAPPORT-2004/03860

FORSVARETS FORSKNINGSINSTITUTT
Norwegian Defence Research Establishment
P O Box 25, NO-2027 Kjeller, Norway

FORSVARETS FORSKNINGSINSTITUTT (FFI)
Norwegian Defence Research Establishment

P O BOX 25
N0-2027 KJELLER, NORWAY

UNCLASSIFIED

SECURITY CLASSIFICATION OF THIS PAGE
(when data entered)

REPORT DOCUMENTATION PAGE

1) PUBL/REPORT NUMBER FFI/RAPPORT-2004/03860 1a) PROJECT REFERENCE FFI-V/860/01	2) SECURITY CLASSIFICATION UNCLASSIFIED 2a) DECLASSIFICATION/DOWNGRADING SCHEDULE -	3) NUMBER OF PAGES 50

4) TITLE

Mechanical studies of wolfram carbide

5) NAMES OF AUTHOR(S) IN FULL (surname first)

Frøyland Øyvind , Moxnes John F

6) DISTRIBUTION STATEMENT

Approved for public release. Distribution unlimited. (Offentlig tilgjengelig)

7) INDEXING TERMS

IN ENGLISH:	IN NORWEGIAN:
a) Mechanical properties	a) Mekaniske egenskaper
b) Fracturing	b) Brudd
c) Yield function	c) Flytefunksjon
d) Wolfram Carbide	d) Wolfram karbid
e) Penetrator	e) Penetrator

THESAURUS REFERENCE:

8) ABSTRACT

In this article a study of the mechanical properties of a sintered wolfram carbide-cobalt penetrator has been carried out. Different penetrators are studied in a compression test to establish the Young’s modulus, the bulk modulus, the yield function and the fracture stress and strain during simple compression. Also the data are used to calculate the fracture strain during simple tension.

In the last section the data are compared with data reported from the literature and some suggestions for increasing the penetration capability of the penetrator are provided.

9) DATE	AUTHORIZED BY This page only	POSITION
2004-11-10	Bjarne Haugstad	Director of Research

ISBN 82-464-0930-1

UNCLASSIFIED

SECURITY CLASSIFICATION OF THIS PAGE
(when data entered)

CONTENTS

Mechanical studies of wolfram carbide

1 INTRODUCTION

Nammo Raufoss AS is the inventor of the Multipurpose (MP) ammunition concept. The MP technology was developed during the end of the 60s and the first series production started in the beginning of the 70s. Still the product is of great importance for the company's medium caliber division. Large volumes of ammunition are delivered for the armed forces around the world and in Norway.

The hard core of the 12.7 mm MP projectile consists of a high-density Wolfram Carbide-Cobalt (WC-Co) hardmetal. The penetration capabilities of the hard core are of cause strongly dependent of the material properties. Of special interest is the tensile and compressive strength of this hard metal, which is very attractive. The greatest limitation when using hard metals materials is the in general low ductility in comparison to for instance some steel materials. Thus when the stresses during reaches the fracture surface the low ductility enhance a fast decrease in the strength due to damage. For steel materials the strength stays high for much larger plastic strains due to the in general larger ductility.

During penetration the compressive strength of the hardcore is the most important quantity, while during exit of a target the tensile strength is more important. In general the best penetrator is one that does not fracture during impact and penetration, but fractures during exit. When the hardcore fractures during exit the number of fragments increases and in general enhances damage to the structure behind the armour. During exit the tensile strength is the most important material parameter.

The parameters established for the different hard cores are

- Young's modulus
- Compressive modulus
- Yield function as a function of effective strain
- Pressure function as a function volumetric strain
- Fracture stress and fracture strain during simple compression

Also by using a curve fitting procedure to the experimental data and by using the transverse rupture stress from the literature we also calculate the

- The maximum yield stress and the strain when the yield function first reached the maximum value
- The fracture stress and fracture strain during simple extension

Other tests that gives important material parameters are the bending test and the hardness test. These test are only slightly discussed in this article.

2 THE EXPERIMENTAL SET UP DURING SIMPLE COMPRESSION

The set up of the compression test is shown in figure 2.1.

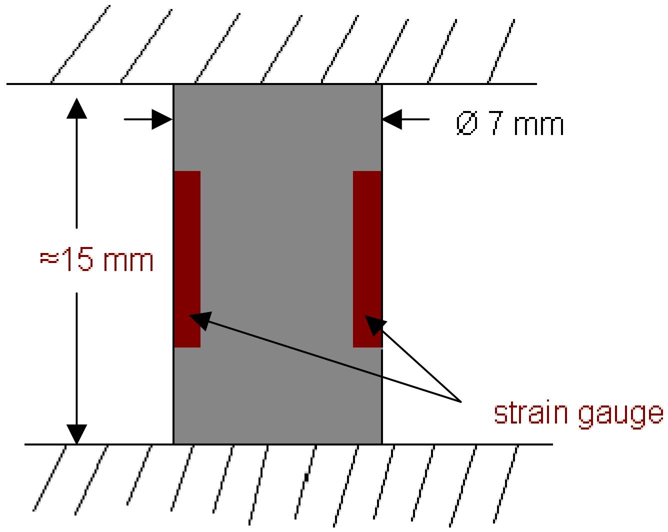

Figure 2.1: Set up of compression test.

Figure 2.2: The hardmetal test specimen after fracture.

The experimental recordings were the force and the longitudinal strain of the cylindrical test specimen. The test specimen was cut out from the hard core by a precision cut-off machine.

During compression two strain gauges were placed on the opposite sides of the hardmetal cylinder to measure the longitudinal strain. Thereafter the strain was calculated as the average of the two recordings (figure 2.4 and 2.6). By doing this we could control any displacement of the cylinder away from the longitudinal direction. For some recordings the difference between the two gauges was small (figure 2.4) and for some the differences between the two gauges were larger (figure 2.6). By comparing the average value with results from other identical cylinders (figure 2.7), we found that the average strain value is a good approximation to the true longitudinal strain for the cylinder. The figures below shows the actual data output from the force sensor and strain gauges.

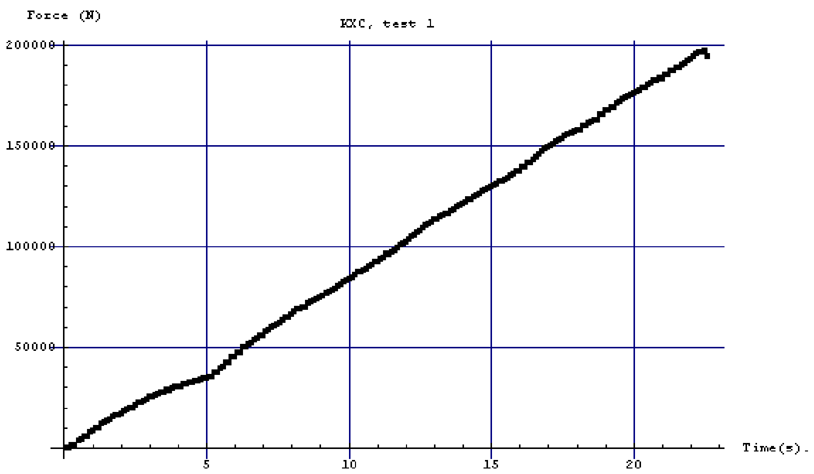

Figure 2.3: Force versus time.

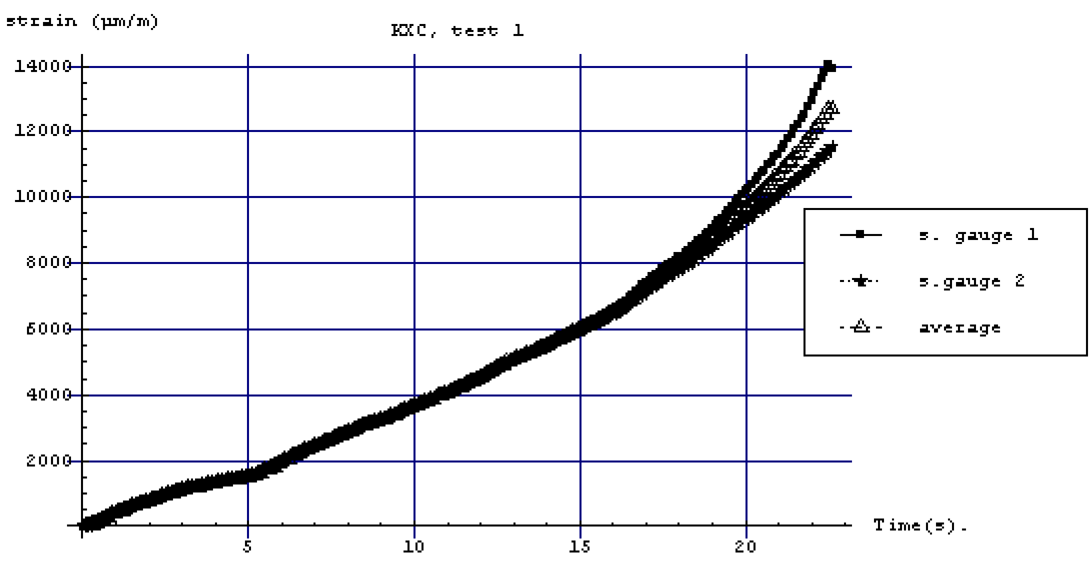

Figure 2.4: Strain versus time.

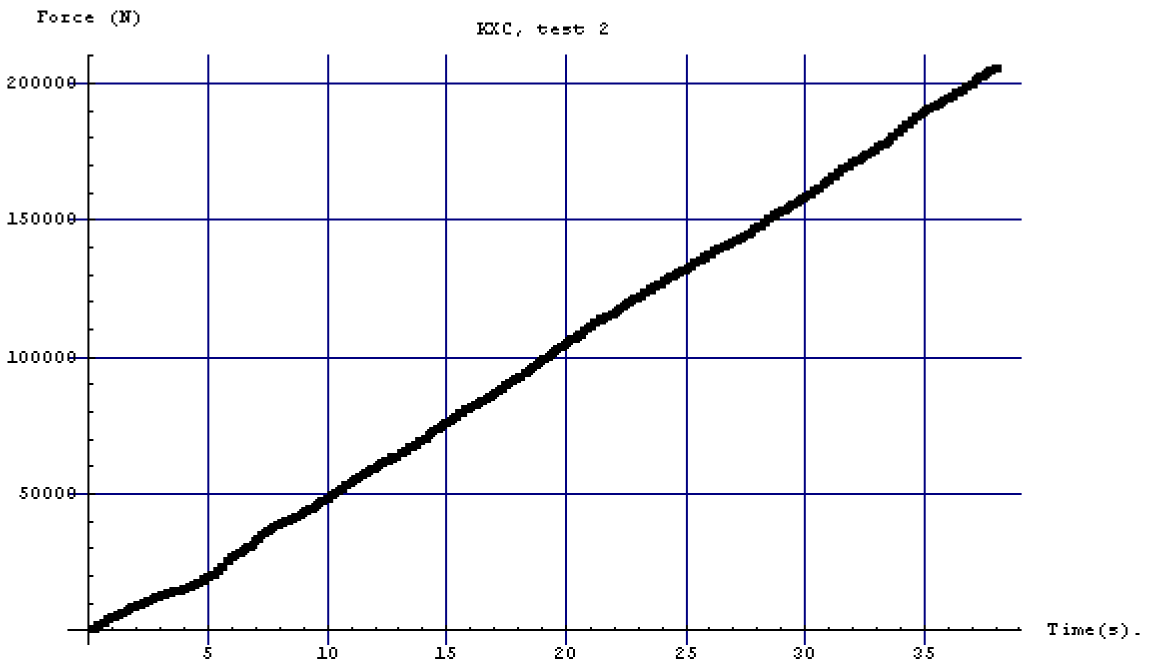

Figure 2.5: Force versus time.

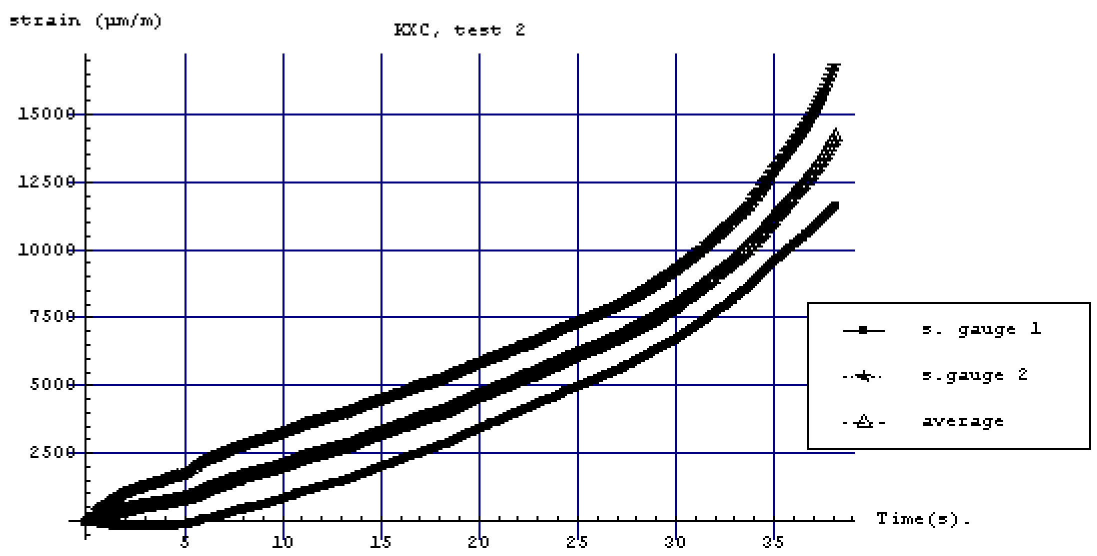

Figure 2.6: Strain versus time.

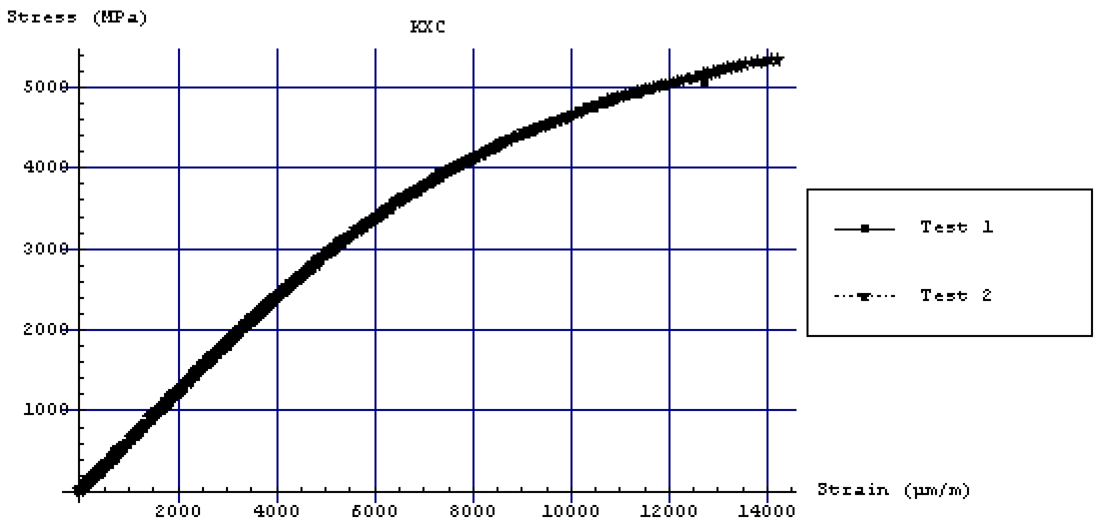

Figure 2.7: Compressive stress versus strain.

Figure (2.2) shows the fragments of the test specimen after fracturing. We observe that the numbers of fragments are large. This indicates that the actual seeds for the unstable crack growths were large. Basically this indicates that the numbers of seeds are so large that increasing the dimension of the test specimen should not influence the results significantly. This suggests that the Weibull modulus is large (10-20).

Different tests were averaged and fitted to a function of the form

$$\sigma(\varepsilon)=\begin{cases}\dfrac{E\varepsilon}{1+a\,\varepsilon^{n}},\ when\ \varepsilon\le\varepsilon_{top}=\left(\dfrac{1}{na-a}\right)^{\frac{1}{n}}\\ \sigma_{top}=\dfrac{E\varepsilon_{top}}{1+a\,\varepsilon_{top}{}^{n}},\ when\quad \varepsilon\le\varepsilon_{top}\end{cases}\tag{2.1}$$

where ε_{top} is the maximum point of the yield function also given by $\partial\sigma(\varepsilon)/\partial\varepsilon=0,\ when\ \varepsilon=\varepsilon_{top}$. It will be shown that the least square fit was excellent. During simple compression the hardcore fractured before the yield function reached the maximum value and the fitted function was accordingly used for extrapolation to find the maximum yield stress and the strain when the yield function reached the upper level. These values are important parameters for other more general types of loadings where the pressure is larger compared to the Missies stress. We also estimated the initial yield point and the corresponding strain by using a 2% offset of the "effective" Young's modulus, i.e. we used that

$$\sigma(\varepsilon)=Y=\frac{E\varepsilon}{1+a\,\varepsilon^{n}}=0.98E\varepsilon\Rightarrow\varepsilon=\varepsilon_{y}=\left(0.02/a\right)^{1/n},Y=\frac{E\varepsilon_{y}}{1+a\,\varepsilon_{y}{}^{n}}\tag{2.2}$$

Finally the fracture strain during simple tension was calculated by using the literature value for the transverse rupture strength (TRS) as the strength during simple tension. To read

$$\sigma(\varepsilon)=\frac{E\varepsilon}{1+a\,\varepsilon^n}=TRS\Rightarrow\varepsilon_{tf}\approx\frac{TRS}{E}\left(1+a\left(\frac{TRS}{E}\right)^n\right) \tag{2.3}$$

where ε_{tf} is the calculated fracture strain during simple tension.

The plastic surface model is assumed to be of the form

$$\begin{gathered}\sigma^m\left(e^m\right)\overset{mod}{=}F\left(e^m\right),\sigma^m\overset{def}{=}\left(\frac{3}{2}S_{ij}{}^2\right)^{1/2},\ e^m\overset{def}{=}\left(\frac{2}{3}e_{ij}{}^2\right)^{1/2},\\ S_{ij}\overset{def}{=}\sigma_{ij}-\frac{1}{3}\delta_{ij}\sigma_{kk},\ e_{ij}\overset{def}{=}\varepsilon_{ij}-\frac{1}{3}\delta_{ij}\varepsilon_{kk},\end{gathered} \tag{2.4}$$

where σ^m is the familiar equivalent stress , e^m is the equivalent strain and F is the flow relation. During a simple compression we achieve that

$$\begin{gathered}\sigma_{ij}=0\ for\ i\neq j,\ \sigma_{22}=\sigma_{33}=0,\ \sigma_{11}\leq 0,\\ \varepsilon_{ij}=0\ for\ i\neq j,\ \varepsilon_{22}=\varepsilon_{33},\ \varepsilon_{11}\leq 0,\end{gathered} \tag{2.5}$$

Then it follows from (2.4) and (2.5) that

$$\begin{gathered}S_{11}=\sigma_{11}-\frac{1}{3}\sigma_{11}=\frac{2}{3}\sigma_{11},\ S_{22}=S_{33}=-\frac{1}{3}\sigma_{11}\\ e_{11}=\varepsilon_{11}-\frac{1}{3}\left(\varepsilon_{11}+2\varepsilon_{22}\right),\ e_{22}=e_{33}=-\frac{1}{2}e_{11}\end{gathered} \tag{2.6}$$

This gives when inserting into (2.4) that

$$\sigma^m=\left|\sigma_{11}\right|,\ e^m=\left|e_{11}\right| \tag{2.7}$$

Thus unless the material is incompressible the axial stress must be plotted against the reduced axial strain e_{11} to reveal the plastic yield surface.

For a linear elastic material it is easy to derive the following equation

$$S_{ij}=2Ge_{ij} \tag{2.8}$$

Inserting into the definition in (2.4) gives that

$$\sigma^m\overset{def}{=}\left(\frac{3}{2}S_{ij}{}^2\right)^{1/2}=3Ge^m \tag{2.9}$$

Thus by plotting the axial stresses against the axial reduced strain the shear modulus G is revealed during simple compression since $\sigma^m = |\sigma_{11}|$ and $e^m = |e_{11}|$.

Finally we study the Poisson's ratio. Define the total ratio and the elastics ration during simple compression as

$$\begin{aligned} \nu^t &\overset{def}{=} -\frac{\varepsilon_{22}}{\varepsilon_{11}} = -\frac{\varepsilon_{33}}{\varepsilon_{11}}, \ (a) \\ \nu &\overset{def}{=} -\frac{\varepsilon^e{}_{22}}{\varepsilon^e{}_{11}} = -\frac{\varepsilon^e{}_{33}}{\varepsilon^e{}_{11}}, \ (b) \end{aligned} \tag{2.10}$$

where the superscript "t" means the total Poisson ratio. Assuming that the volumetric plastic deformation is insignificant i.e. $\varepsilon_{kk} = \varepsilon^p{}_{kk} + \varepsilon^e{}_{kk} = \varepsilon^e{}_{kk}$, we further have for a linear elastic part when using (2.10a)

$$\begin{aligned} \sigma_{11} &= 3K\left(\varepsilon^e{}_{11} + \varepsilon^e{}_{22} + \varepsilon^e{}_{33}\right) = \frac{E}{1-2\nu}\left(\varepsilon^e{}_{11} + \varepsilon^e{}_{22} + \varepsilon^e{}_{33}\right) \\ &= 3K\left(\varepsilon_{11} + \varepsilon_{22} + \varepsilon_{33}\right) = 3K\left(1-2\nu^t\right)\varepsilon_{11} = \frac{E}{1-2\nu}\left(1-2\nu^t\right)\varepsilon_{11} \end{aligned} \tag{2.11}$$

(2.11) can be solved for the total Poisson's ratio to give the equation

$$\nu^t = \frac{1}{2} - \left(\frac{1}{2} - \nu\right)\frac{\sigma_{11}}{E\varepsilon_{11}} \tag{2.12}$$

It also follows that

$$\varepsilon_{11} + \varepsilon_{22} + \varepsilon_{33} = \varepsilon_{11} + 2\varepsilon_{22} = \varepsilon_{11}\left(1-2\nu^t\right) = \left(1-2\nu\right)\frac{\sigma_{11}}{E} \tag{2.13}$$

Then it follows that

$$e_{11} = \varepsilon_{11} - \frac{1}{3}\left(\varepsilon_{11} + 2\varepsilon_{22}\right) = \varepsilon_{11} - \left(1-2\nu\right)\frac{\sigma_{11}}{3E} \tag{2.14}$$

Since most materials do not vary so much in the elastic Poisson's ratio, equation (2.14) can be used to transform between the axial strain and the reduced axial strain.

3 THE COMPRESSION TEST

The compression test is used to establish a relation for the material parameters. The test did not correspond to the ISO standard, but we show that the recorded values are in good agreement with the ISO standard values in cases were we could compare the results.

3.1 KMS (Kennametal Hertel)

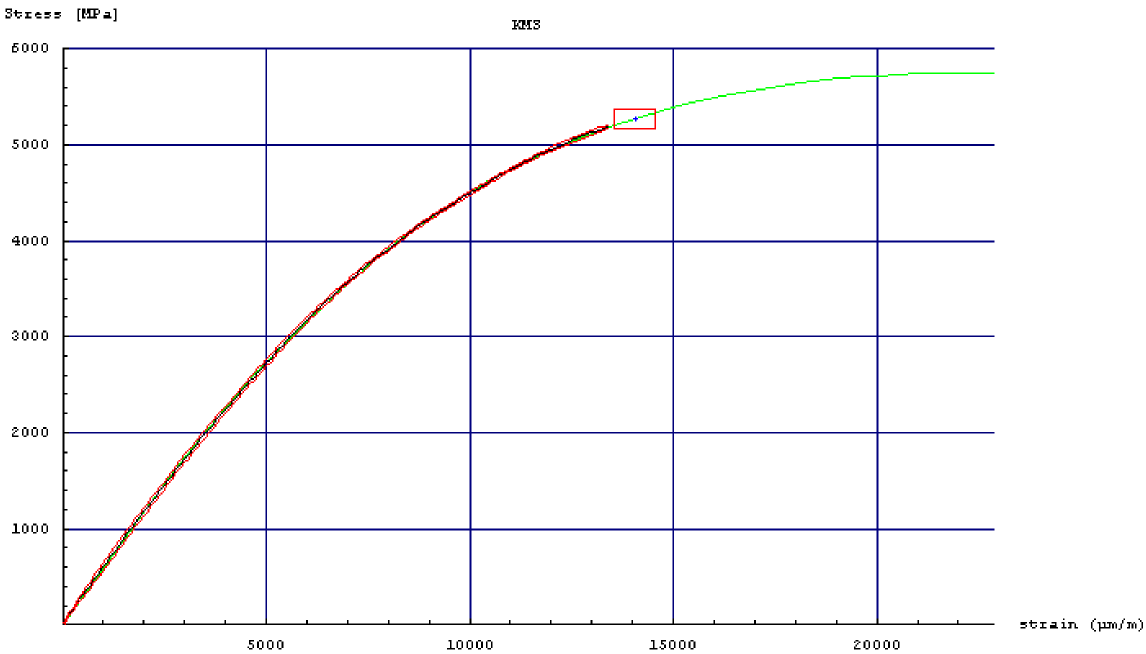

— Average of the measurements • Average measured fracture point — Standard deviation of the measurements
— Fit function

Figure 3.1: Compressive stress versus longitudinal strain.

The average of the measurements are based upon four different tests. The function that give least square fit to the average of the measurements are:

$$\sigma(\varepsilon) = \frac{E\varepsilon}{1 + a\,\varepsilon^n} = \frac{0.600971\ \varepsilon}{1 + 4.4105 \cdot 10^{-8}\ \varepsilon^{1.72}}$$

,where σ is in MPa, E is in TPa, ε in µm/m and a and n is nondimensional constants.

$\sigma(\varepsilon)$ reached the maximum for:

$\varepsilon_{top} = 22877$ µm/m, $\sigma_{top} = 5755$ MPa.

The exerimental values for the average of the fracture point is:

$\overline{\varepsilon}_f = 14065$ µm/m, $\overline{\sigma}_f = 5269$ MPa.

We observe that the fitted function goes close through the experimental values for the fracture point. This is not obvious since the fitted function was only fitted to the data where all the test specimens were not fractured. This point is below the average measured fracture point. Also observe that the fracture stress is not close to the maximum stress that can be reached for other types of loadings.

3.2 KXC (Kennametal Hertel)

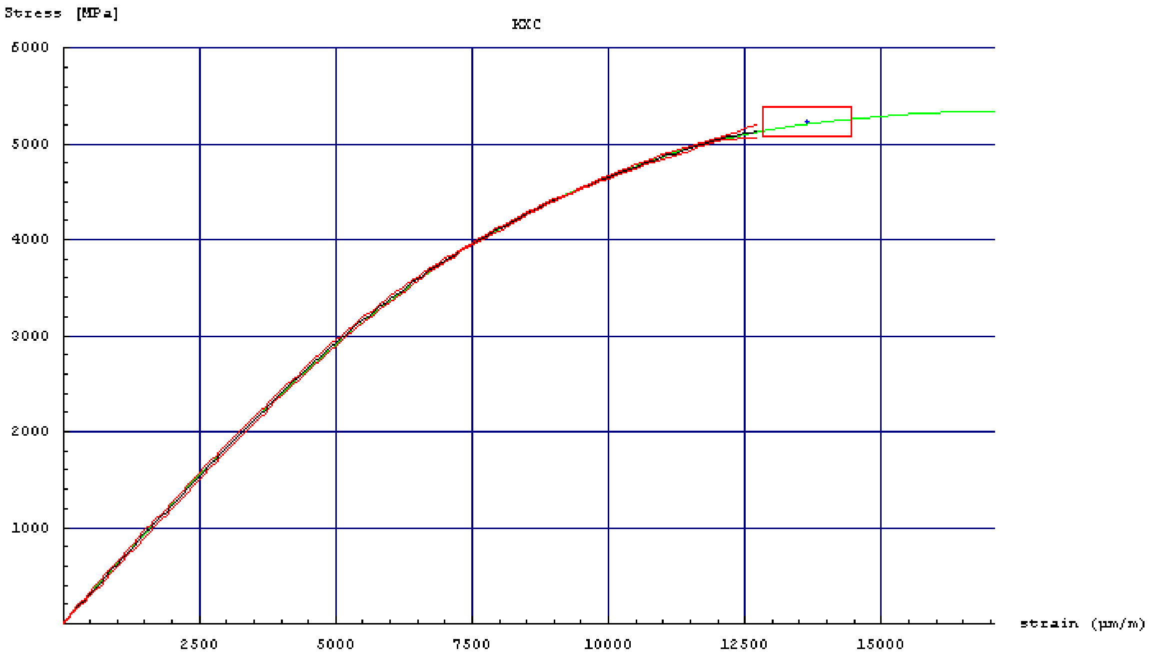

— Average of the measurements • Average measured fracture point — Standard deviation of the measurements

— Fit function

Figure 3.2: Compressive stress versus longitudinal strain.

The average of the measurements are based upon three different tests. The function that gives least discrepancy from the average of the measurements are:

$$\sigma(\varepsilon) = \frac{E\varepsilon}{1+a\,\varepsilon^{n}} = \frac{0.634632\ \varepsilon}{1+4.73849\cdot 10^{-9}\ \varepsilon^{1.97}}$$

,where σ is in MPa, E in TPa, ε in μm/m and a and n is nondimensional constants.

$\sigma(\varepsilon)$ reached the maximum for:

$\varepsilon_{top} = 17071$ μm/m, $\sigma_{top} = 5334$ MPa.

The experimental values for the average of the fracture point is:

$\bar{\varepsilon}_f = 13640$ μm/m, $\bar{\sigma}_f = 5231$ MPa.

We observe that the fitted function goes close through the experimental values for the fracture point. Also observe that the fracture stress is close to the maximum stress that can be reached for other types of loadings.

3.3 G10 (Kennametal Hertel)

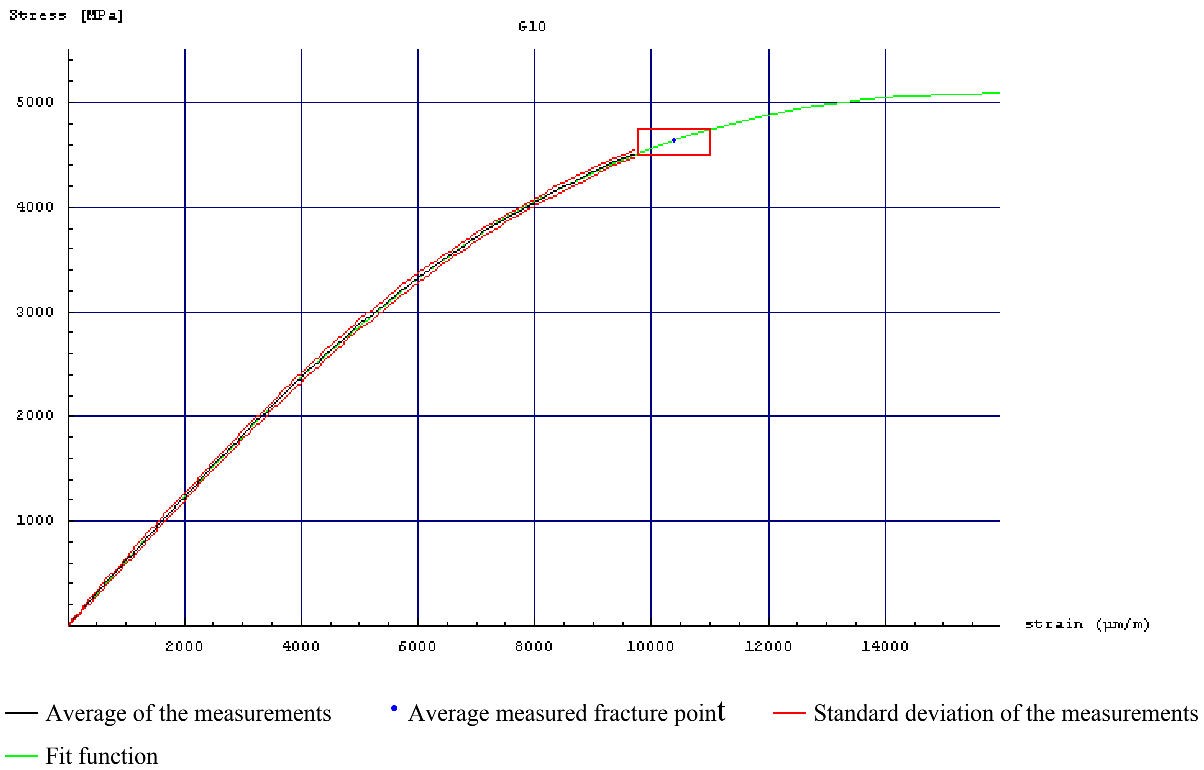

Figure 3.3: Compressive stress versus longitudinal strain.

The average of the measurements are based upon three different tests. The function that gives the least discrepancy from the average of the measurements are:

$$\sigma(\varepsilon) = \frac{E\varepsilon}{1 + a\,\varepsilon^n} = \frac{0.625768\ \varepsilon}{1 + 2.5677 \cdot 10^{-9}\ \varepsilon^{2.04}}$$

,where σ is in MPa, E in TPa, ε in µm/m and a and n is nondimensional constants.

$\sigma(\varepsilon)$ has a maximum for:

$\varepsilon_{top} = 15946$ µm/m, $\sigma_{top} = 5087$ MPa.

The experimental values for the average of the fracture point is:

$\overline{\varepsilon}_f = 10382$ µm/m, $\overline{\sigma}_f = 4628$ MPa.

For this WC-Co hardmetal we also measured the circumferential strain, $\varepsilon_{\theta\theta}$, on one specimen. A strain gauge was mounted on each side of the specimen. Because of the small size of the test specimen there was no space left to mount any strain gauges in the longitudinal direction. Therefore we simply took the longitudinal strain, ε_{zz}, from one of the tests we already had measured and used this to get the volumetric strain. Although we did not measure the longitudinal and circumferential strain on the same specimen we believe the volumetric strain is truthful.

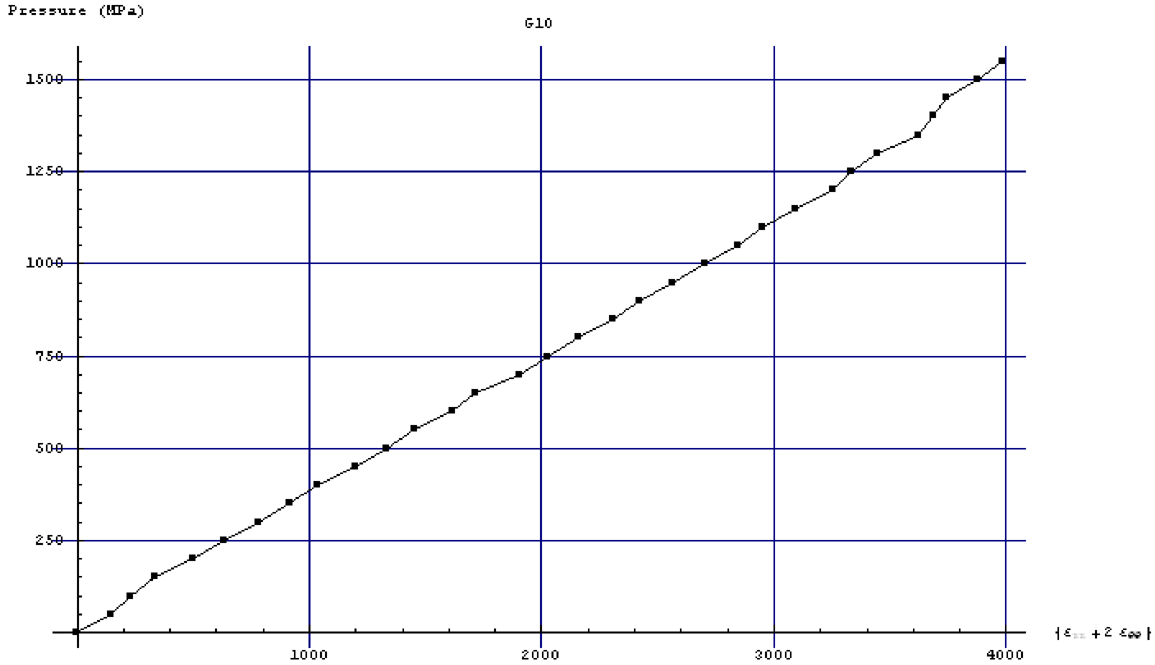

Figure 3.4: Pressure [MPa] versus volumetric strain [µm/m].

The bulk modulus, K, is the slope for the first part of the curve in figure 3.4. Since our curve is almost linear up to 2000 µm/m, we fitted a linear function in the range 0 – 2000 µm/m. This gives K=375.7 GPa. Thus the elastic Poisson ration is $1/2-\left(E/6K\right)=0.22$.

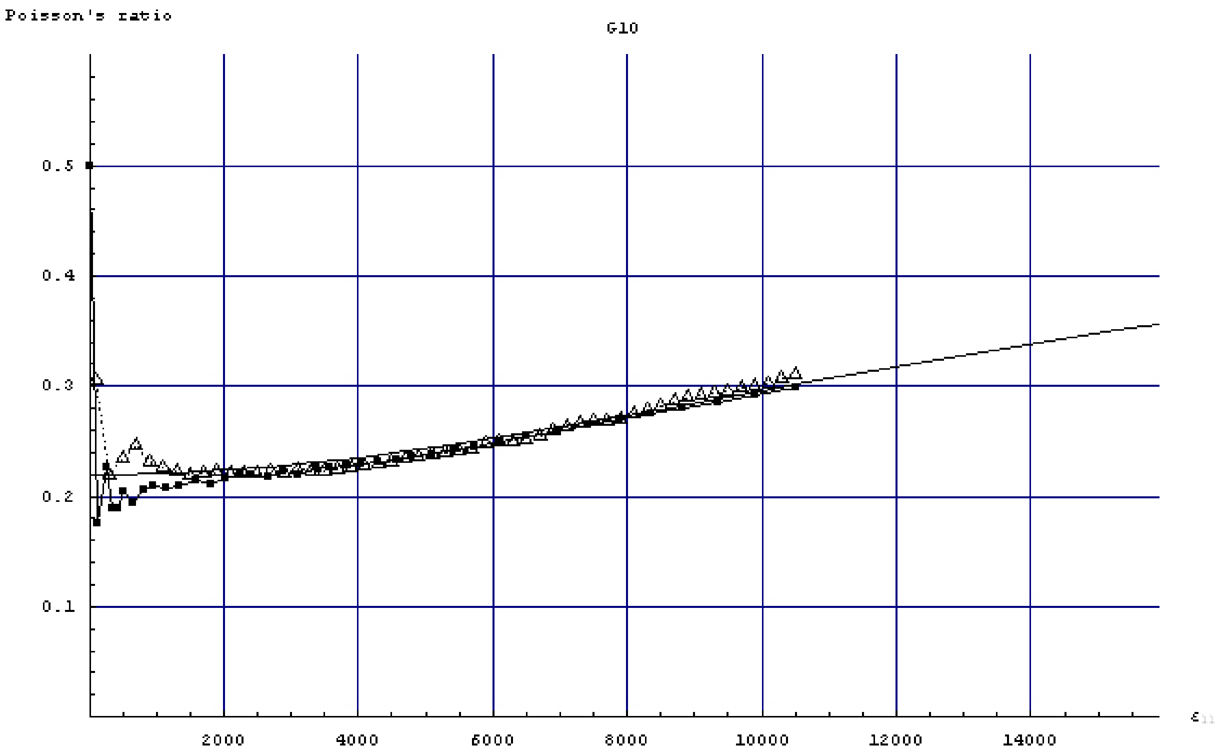

— Analytical solution of Eqn. 2.12 Δ $\varepsilon_{\theta\theta}/\varepsilon_{zz}$ for the experiment ▪ Experimental values in Eqn. 2.12

Figure 3.5: The total Poisson's ratio (ν) as a function of the longitudinal strain (ε_{zz} [µm/m]).

3.4 H8N (Sandvik Hard Material)

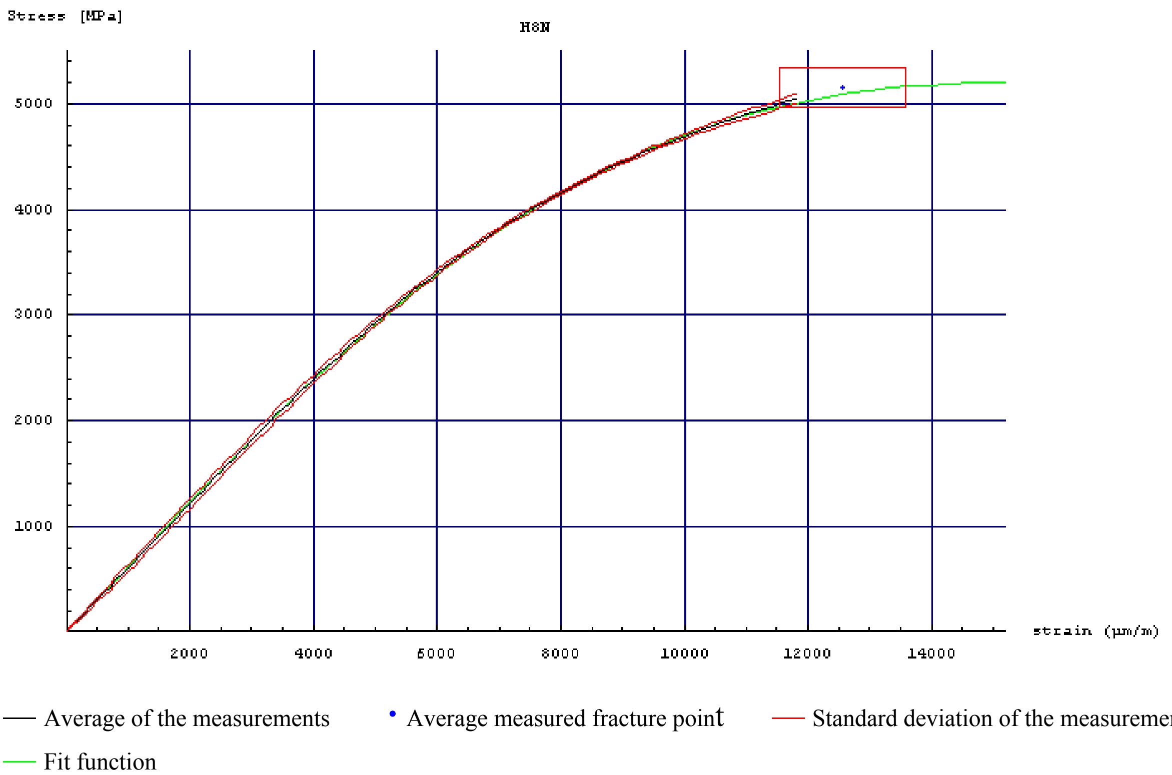

Figure 3.6: Compressive stress versus longitudinal strain.

The average of the measurements are based upon three different tests. The function that gives the least discrepancy from the average of the measurements are:

$$\sigma(\varepsilon) = \frac{E\varepsilon}{1 + a\,\varepsilon^{n}} = \frac{0.622831\ \varepsilon}{1 + 4.26607 \cdot 10^{-10}\ \varepsilon^{2.22}}$$

,where σ is in MPa, E in TPa, ε in µm/m and a and n is nondimensional constants.

$\sigma(\varepsilon)$ reached the maximum for:

$\varepsilon_{top} = 15199$ µm/m, $\sigma_{top} = 5202$ MPa.

The experimental values for the average of the fracture point is:

$\overline{\varepsilon}_f = 12561$ µm/m, $\overline{\sigma}_f = 5154$ MPa.

3.5 H6N (Sandvik Hard Material)

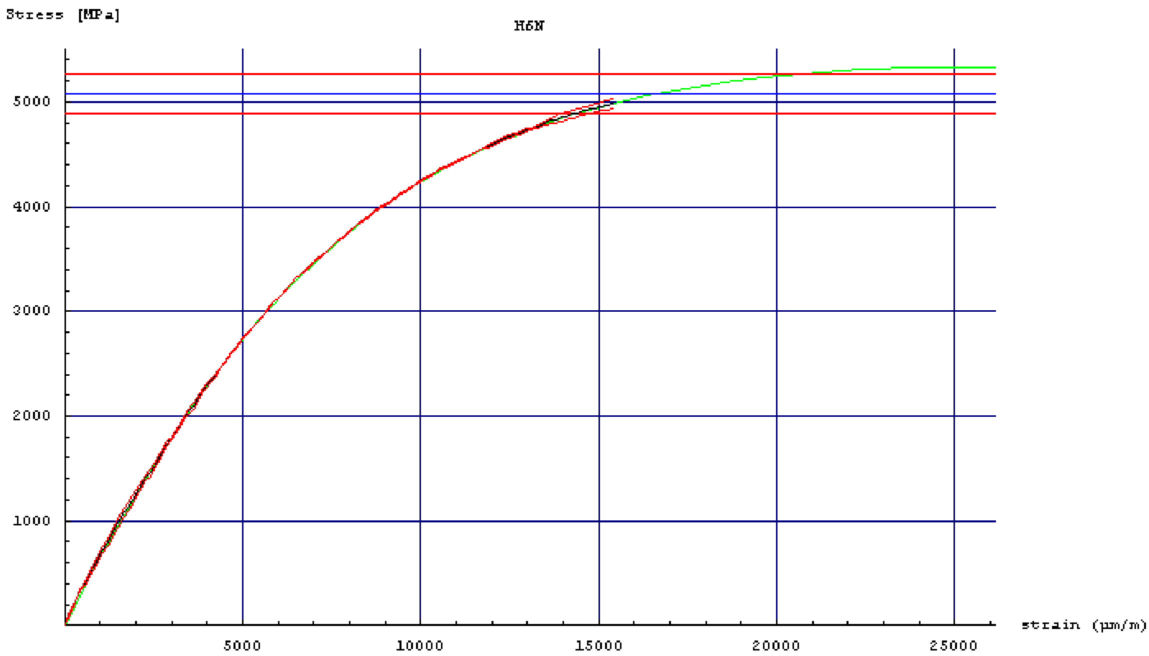

— Average of the measurements — Average fracture stress — Standard deviation of the fracture stress

— Fit function

Figure 3.7: Compressive stress versus longitudinal strain.

The average of the measurements are based upon two different tests. In one of the tests the strain signal was lost before reaching the fracture point. This is due to limitation of the software/amplifier we used. Thus, there are no valid average or standard deviation for the strain measurements at the fracture point. However, we assumed that the average fracture strain is at the intersection for the average fracture stress and the fitted function. The function that gives the least discrepancy from the average of the measurements are:

$$\sigma(\varepsilon) = \frac{E\varepsilon}{1 + a\,\varepsilon^n} = \frac{0.657763\ \varepsilon}{1 + 8.74275 \cdot 10^{-7}\ \varepsilon^{1.45}}$$

,where σ is in MPa, E in TPa, ε in µm/m and a and n are nondimensional constants.

$\sigma(\varepsilon)$ reached the maximum for:

$\varepsilon_{top} = 26142$ µm/m, $\sigma_{top} = 5336$ MPa.

The average compressive stress at the fracture point is measured

$\overline{\sigma}_f = 5080$ MPa

Intersection point between average fracture stress and the function $\sigma(\varepsilon)$ gives:

$\rightarrow\ \varepsilon(\overline{\sigma}_f) = 16631$ µm/m.

3.6 H10N (Sandvik Hard Material)

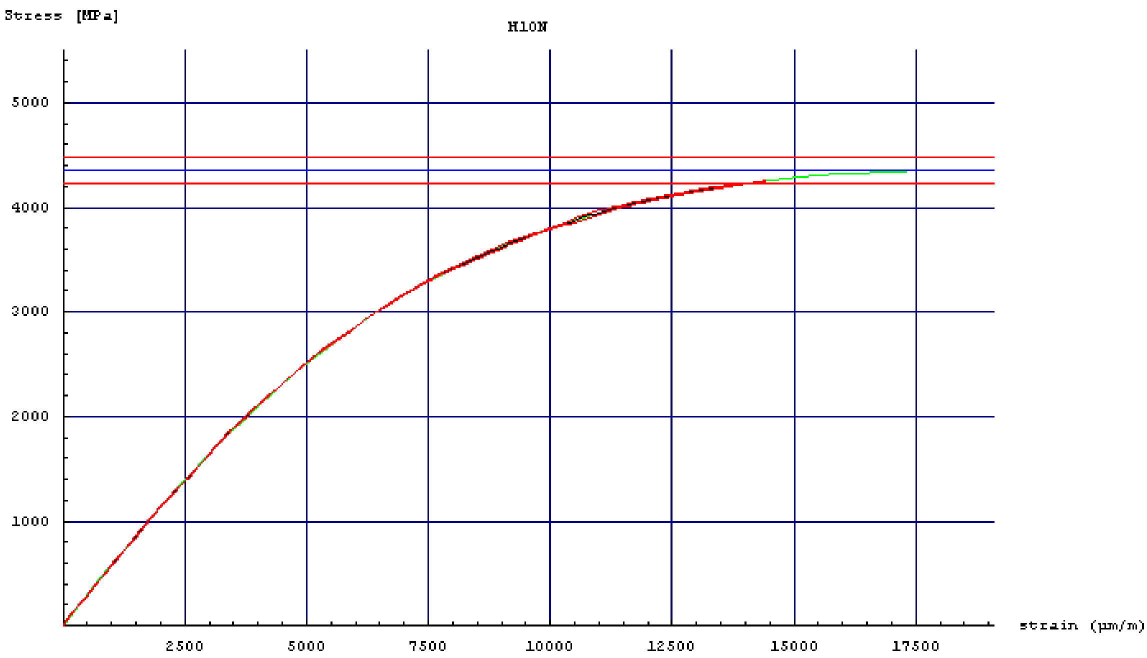

— Average of the measurements — Average fracture stress — Standard deviation of the fracture stress

— Fit function

Figure 3.8: Compressive stress versus longitudinal strain.

The average of the measurements are based upon three different tests. In one of the tests the strain signal was lost before reaching the fracture point. This is due to limitation of the software/amplifier we used. Thus, there are no valid average or standard deviation for the strain measurements at the fracture point. However, we assumed that the average fracture strain is at the intersection for the average fracture stress and the function. The function that gives the least discrepancy from the average of the measurements are:

$$\sigma(\varepsilon) = \frac{E\varepsilon}{1 + a\,\varepsilon^n} = \frac{0.591082\ \varepsilon}{1 + 1.6711 \cdot 10^{-7}\ \varepsilon^{1.63}}$$

,where σ is in MPa, E in TPa, ε in µm/m and a and n are nondimensional constants.

$\sigma(\varepsilon)$ reached the maximum for:

$\varepsilon_{top} = 19089$ µm/m, $\sigma_{top} = 4360$ MPa.

The average compressive stress at the fracture point is:

$\overline{\sigma}_f = 4351$ MPa

Intersection point between average fracture stress and the function $\sigma(\varepsilon)$ gives:

$\rightarrow\ \varepsilon(\overline{\sigma}_f) = 17544$ µm/m.

3.7 G15 (Kennametal Hertel)

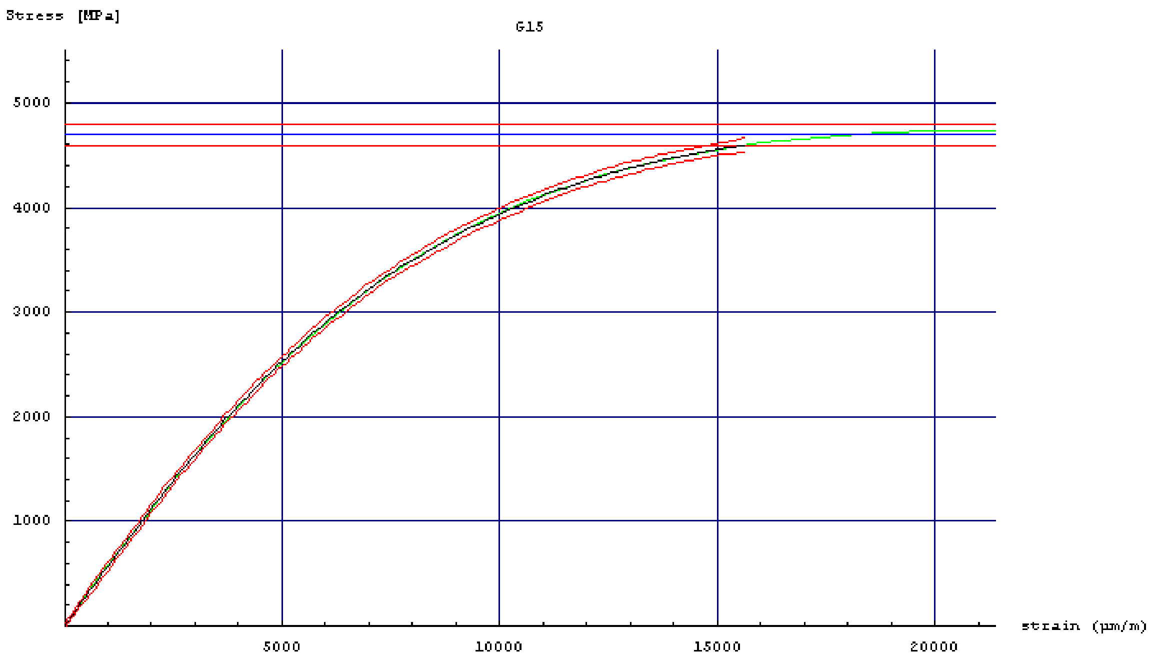

— Average of the measurements — Average fracture stress — Standard deviation of the fracture stress

— Fit function

Figure 3.9: Compressive stress versus longitudinal strain.

The average of the measurements are based upon four different tests. In all the tests the strain signal was lost before reaching the fracture point. This is due to limitation of the software/amplifier we used. Thus, there are no valid average or standard deviation for the strain measurements at the fracture point. However, we assumed that the average fracture strain would be at the intersection for the average fracture stress and the function. The function that gives the least discrepancy from the average of the measurements are:

$$\sigma(\varepsilon) = \frac{E\varepsilon}{1 + a\,\varepsilon^n} = \frac{0.584536\ \varepsilon}{1 + 1.75133 \cdot 10^{-7}\ \varepsilon^{1.61}}$$

,where σ is in MPa, E in TPa, ε in µm/m and a and n are nondimensional constants.

$\sigma(\varepsilon)$ reached a maximum for:

$\varepsilon_{top} = 21380$ µm/m, $\sigma_{top} = 4735$ MPa.

The average compressive stress at the fracture point is:

$\overline{\sigma}_f = 4698$ MPa

Intersection point between average fracture stress and the function $\sigma(\varepsilon)$ gives:

$\rightarrow\ \varepsilon(\overline{\sigma}_f) = 18240$ µm/m.

3.8 Lot 84, unit no. 24 (Baldonit)

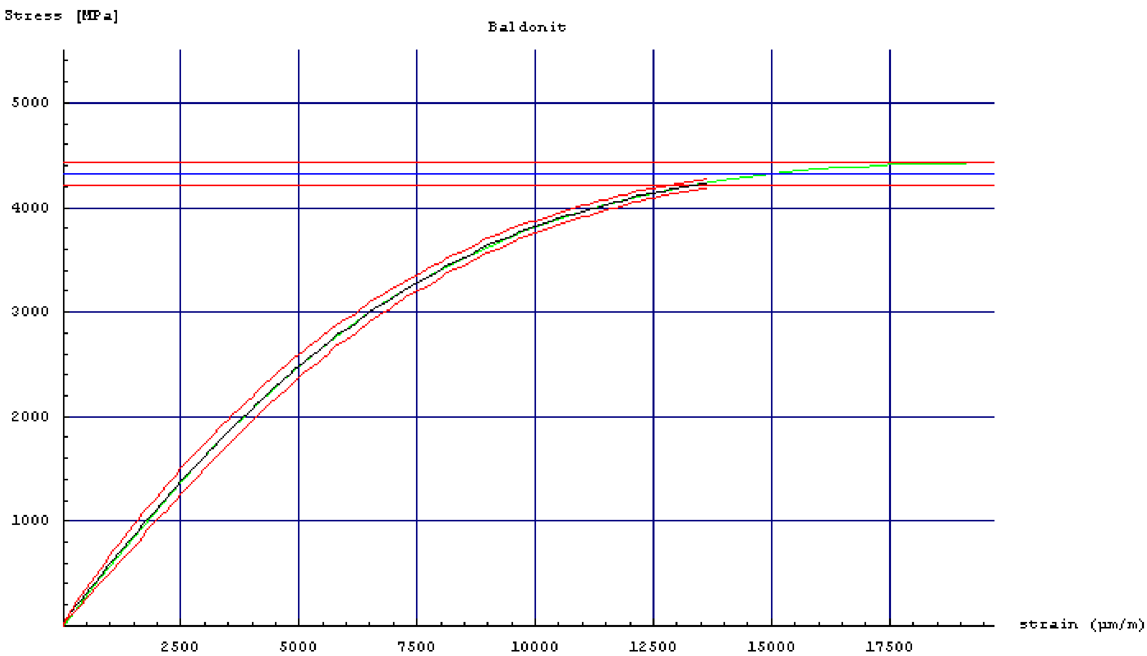

— Average of the measurements — Average fracture stress — Standard deviation of the fracture stress

— Fit function

Figure 3.10: Compressive stress versus longitudinal strain.

The average of the measurements are based upon three different tests. In one of the tests the strain signal was lost before reaching the fracture point. This is due to limitation of the software/amplifier we used. Thus, there are no valid average or standard deviation for the strain measurements at the fracture point. However, we assumed that the average fracture strain would be at the intersection for the average fracture stress and the function. The function that gives the least discrepancy from the average of the measurements are:

$$\sigma(\varepsilon) = \frac{E\varepsilon}{1 + a\,\varepsilon^{n}} = \frac{0.581745\ \varepsilon}{1 + 1.58968 \cdot 10^{-7}\ \varepsilon^{1.63}}$$

,where σ is in MPa, E in TPa, ε in µm/m and a and n are nondimensional constants.

$\sigma(\varepsilon)$ reached a maximum for:

$\varepsilon_{top} = 19683$ µm/m, $\sigma_{top} = 4426$ MPa.

The average compressive stress at the fracture point is:

$\overline{\sigma}_f = 4323$ MPa

Intersection point between average fracture stress and the function $\sigma(\varepsilon)$ gives:

$\varepsilon(\overline{\sigma}_f) = 15035$ µm/m.

3.9 Job number: 13900005, Manufacturing source: 945922 (Cime Bocuze)

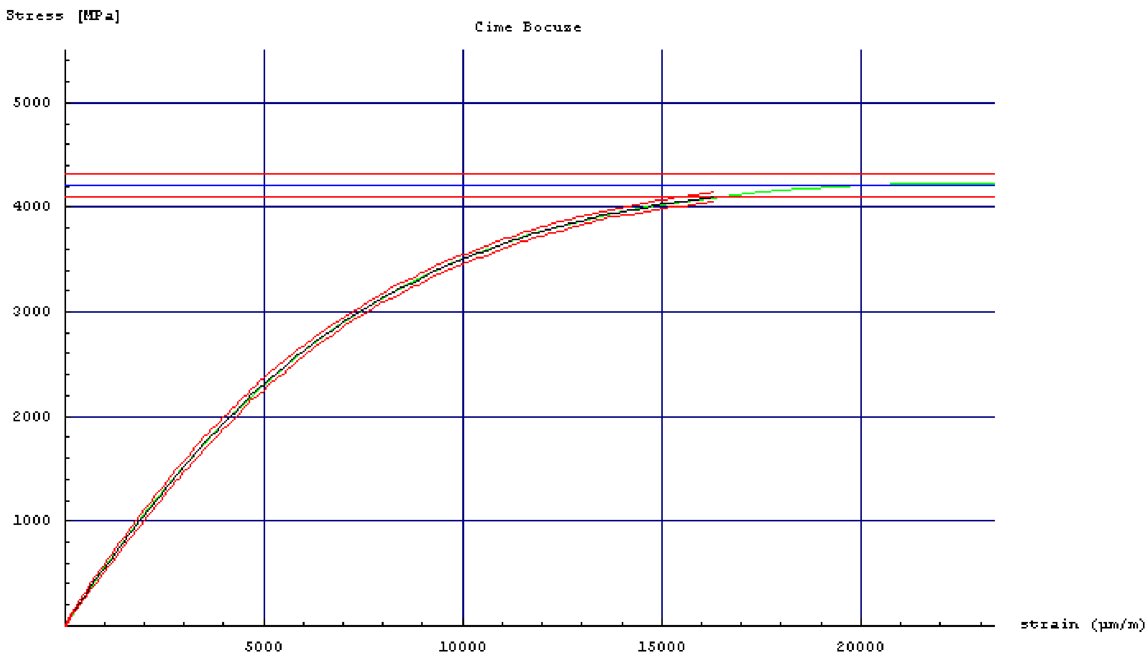

— Average of the measurements — Average fracture stress — Standard deviation of the fracture stress

— Fit function

Figure 3.11: Compressive stress versus longitudinal strain.

The average of the measurements are based upon three different tests. In one of the tests the strain signal was lost before reaching the fracture point. This is due to limitation of the software/amplifier we used. Thus, there are no valid average or standard deviation for the strain measurements at the fracture point. However, we assumed that the average fracture strain would be at the intersection for the average fracture stress and the function. The function that gives the least discrepancy from the average of the measurements are:

$$\sigma(\varepsilon) = \frac{E\varepsilon}{1 + a\,\varepsilon^n} = \frac{0.558617\ \varepsilon}{1 + 7.13379 \cdot 10^{-7}\ \varepsilon^{1.48}}$$

,where σ is in MPa, E in TPa, ε in µm/m and a and n are nondimensional constants.

$\sigma(\varepsilon)$ reached a maximum for:

$\varepsilon_{top} = 23364$ µm/m, $\sigma_{top} = 4233$ MPa.

The average compressive stress at the fracture point is:

$\overline{\sigma}_f = 4206$ MPa

Intersection point between average fracture stress and the function $\sigma(\varepsilon)$ gives:

$\varepsilon(\overline{\sigma}_f) = 19894$ µm/m.

3.10 Summary

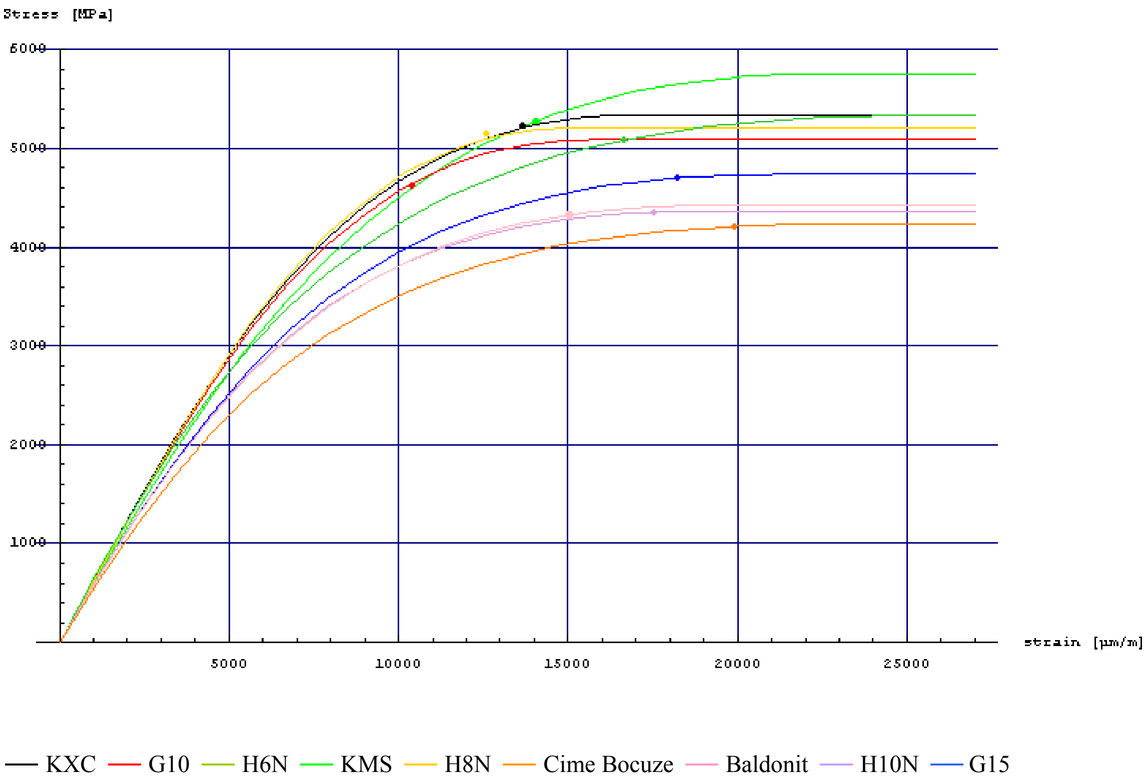

Figure 3.12: Stress versus strain for all tests.

Figure (3.12) shows the results for all tests for the fitted functions. The more general picture that appears is that lower fracture stress is correlated to larger fracture strain. To study this more closely we calculated the energy absorption by using the relation $E = \int_o^{\varepsilon f} \sigma(\varepsilon) d\varepsilon$.

Table (3.1) shows the results. It turns out that the material with lowest fracture stress is able to absorb most energy. The reason is the larger fracture strain. But also G15 is a good candidate.

	Energy [MJ]/m^3	Experimental Compressive Strength [MPa]	Literature Compressive Strength [MPa]	Experimental Fracture strain $[\mu m/m]$	Literature Young's modulus [GPa]	Experimental Young's modulus [GPa]
KMS	45.68	5269+/-101		14065		600
KXC	45.20	5231+/-153		13640		640
G10	28.41	4628+/-122		10382		630
H8N	39.80	5154+/-191	5200	12561	600	620
H6N	56.65	5080+/-188	6200	16631	630	660
H10N	54.42	4351+/-122	5200	17544	585	590
G15	59.83	4698+/-102	4500	18240	580	580
Baldonit	43.57	4323+/-112		15035		580
Cime Bocuze	60.39	4206+/-110		19894		560

Table 3.1: Energy absorption, compressive strength and Young's modulus for the different hard cores.

	Poisson's ratio	Young's modulus, E [TPa]	Bulk modulus, K [TPa]	Shear modulus, G [TPa]	ε_{11f} [μm/m]	ε_{11top} [μm/m]	e_{11f} [μm/m]	e_{11top} [μm/m]	σ_{11f} [MPa]	$\sigma_{11top}(\varepsilon)$ [MPa]	$\sigma_{11top}(e)$ [MPa]	a	n	a'	n'
G10	0.22 [3]	0.6258	0.3725	0.2565	10382	15946	8964	13545	4628	5087	5000	$2.5677\ 10^{-9}$	2.04	$1.26816\ 10^{-8}$	1.92
KMS	0.22 [3]	0.6010	0.3577	0.2463	14065	22877	12416	20329	5269	5755	5691	$4.4105\ 10^{-8}$	1.72	$1.89932\ 10^{-7}$	1.61
KXC	0.22 [3]	0.6346	0.3778	0.2601	13640	17071	12696	14946	5231	5334	5289	$4.73849\ 10^{-9}$	1.97	$2.76399\ 10^{-8}$	1.83
H8N	0.22	0.6228	0.3707	0.2553	12561	15199	11016 [2]	12991	5154	5202	5142	$4.26607\ 10^{-10}$	2.22	$2.85357\ 10^{-9}$	2.07
H6N	0.21	0.6578	0.3915	0.2696	16631 [1]	26142	15325	24847	5080	5336	5319	$8.74275\ 10^{-7}$	1.45	$2.92503\ 10^{-6}$	1.36
H10N	0.22	0.5911	0.3518	0.2422	17544 [1]	19089	16170 [2]	17459	4351	4360	4341	$1.6711\ 10^{-7}$	1.63	$6.85663\ 10^{-7}$	1.52
G15	0.22	0.5845	0.3479	0.2396	18240 [1]	21380	17349	19691	4698	4735	4717	$1.75133\ 10^{-7}$	1.61	$7.23819\ 10^{-7}$	1.5
Baldonit	0.22 [3]	0.5817	0.3463	0.2384	15035 [1]	19683	13871	17992	4323	4426	4403	$1.58968\ 10^{-7}$	1.63	$6.55049\ 10^{-7}$	1.52
Cime Bocuze	0.22 [3]	0.5586	0.3325	0.2289	19894 [1]	23364	18606	22390	4206	4233	4234	$7.13379\ 10^{-7}$	1.48	$2.61302\ 10^{-6}$	1.38

1 – Assumed value for intersection between σ(ε) and σ_f.
2 – The value is calculated using equation 2.14, the other values in this column are calculated using the equation for σ(e) → $e(\sigma_{11f})=e_{11f}$
3 – Assumed value

Table 3.2: Properties for the different WC-Co hardmetals.

For table 3.2 the units is matched to give the values as shown in the table when using the equations $\sigma(e)=\dfrac{3Ge}{1+a'e^{n'}}$ and $\sigma(\varepsilon)=\dfrac{E\varepsilon}{1+a\varepsilon^{n}}$. If using m/m as the unit of the strain instead of μm/m, *a* and *a'* should be multiplied by 10^{6n}, and E and G by 10^6 to give σ in MPa. *n* is unchanged.

The yield strength is an important value since it is the value at which materials starts to show permanent deformation. Because there is no definite point where elastic strain ends and plastic strain starts the yield strength is chosen where the slope of the stress-strain curve deviates 2 percent from the elastic modulus of the hardmetal. The yield strength and corresponding strain is shown in the table below.

	Yield strength [MPa]	Yield strain [μm/m]
G10	1480	2413
KMS	1158	1967
KXC	1450	2331
H8N	1758	2880
H6N	663	1029
H10N	765	1320
G15	803	1402
Baldonit	776	1362
Cime Bocuze	562	1026

Table 3.3: Yield strength and yield strain.

4 OTHER RELATIONS, ALSO SANDVIK DATA

In this section we compare our results with other results from the literature

4.1 Young's modulus as a function of the Cobalt content for different particle sizes

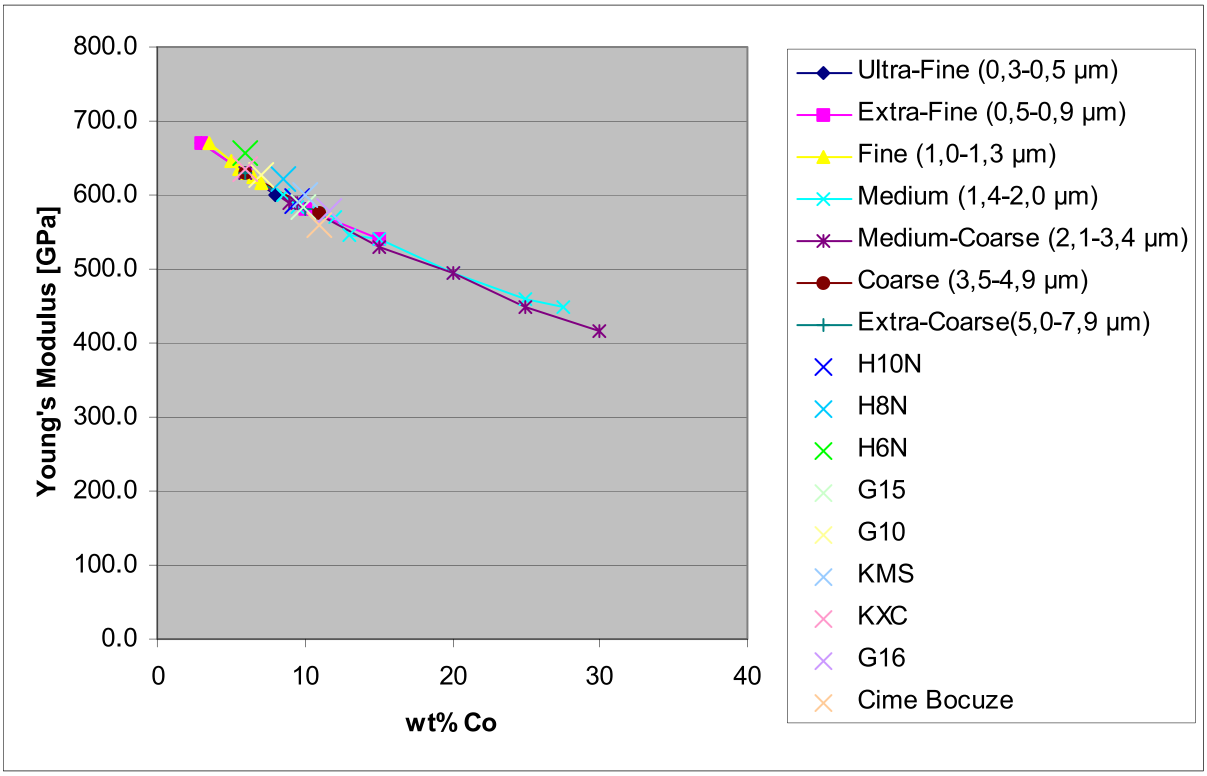

The figure shows that the Young's modulus is not sensitive to the particle size of the WC grains. This shows that elastic deformation is mainly a volumetric property and is only marginally related to surface phenomena in the material.

4.2 Bulk modulus as a function of the Cobalt content for different particle sizes

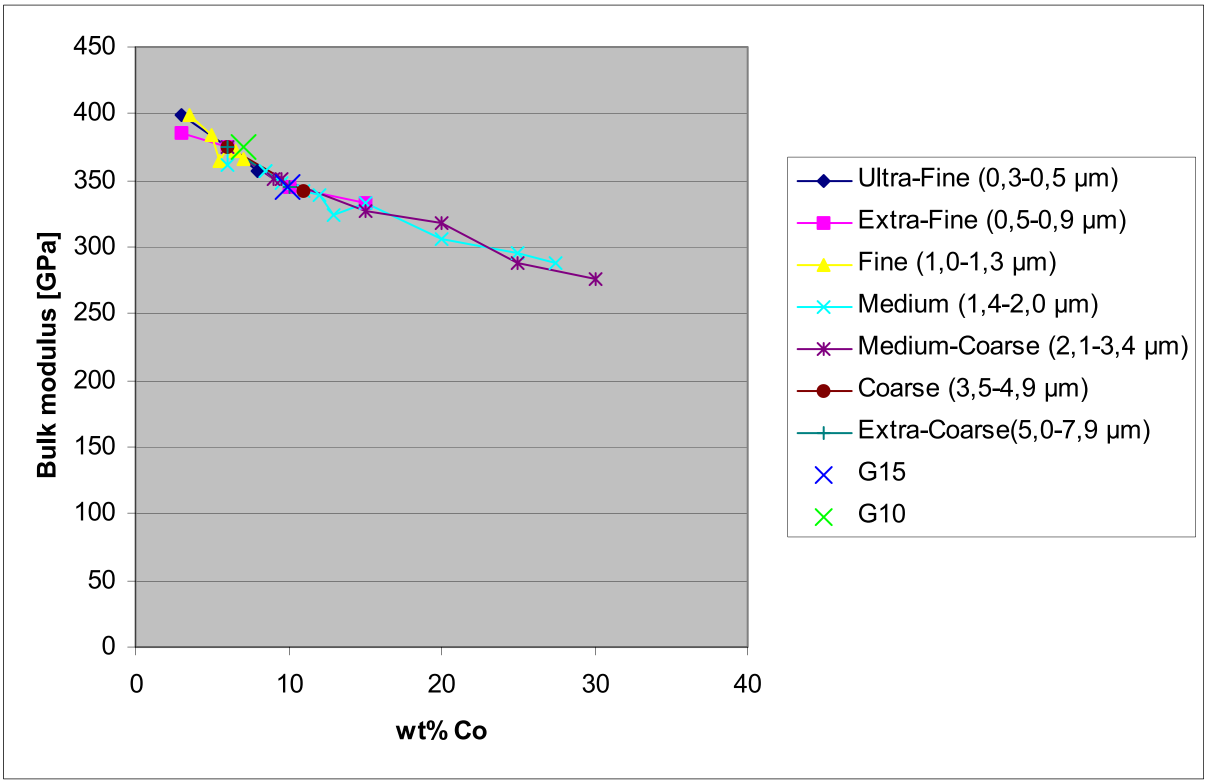

The bulk modulus follows the same kind of relation ship as the Young's modulus. Thereby the Poison ration is only marginally depending on the Co content.

4.3 The plastic parameter a as a function of the Cobalt content

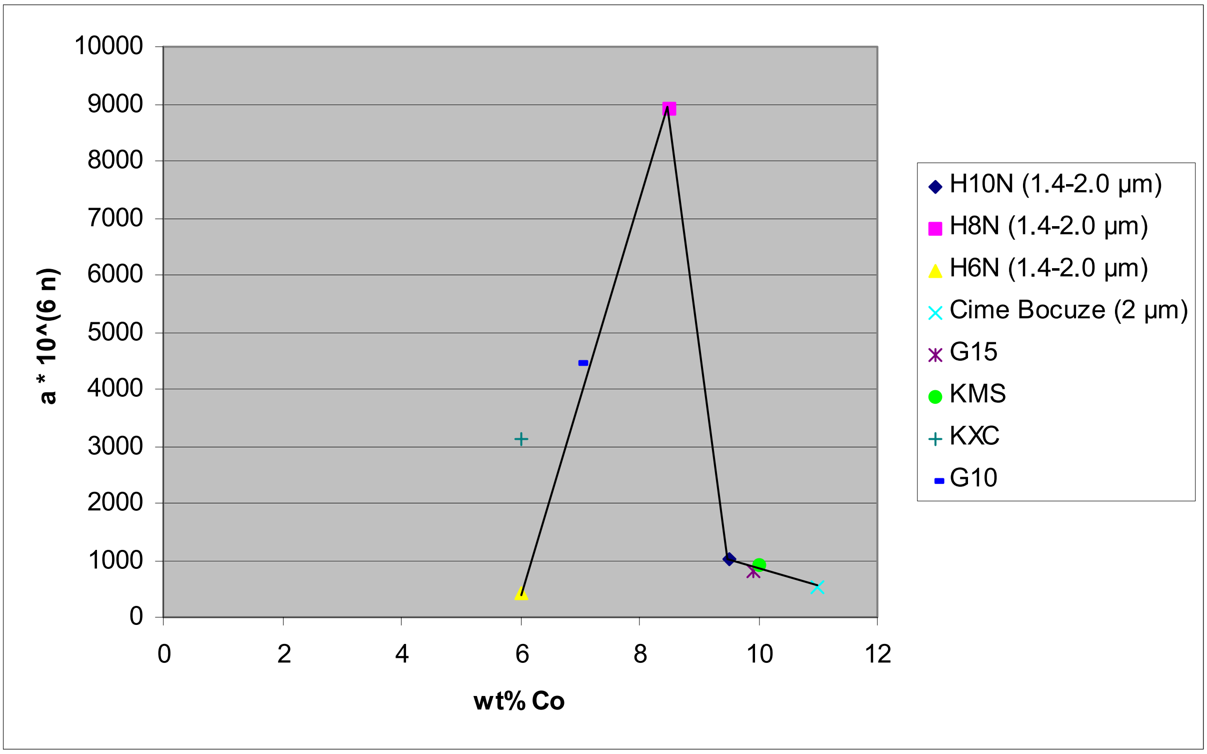

The plastic parameter *a* is here given for strains in m/m. We have only access to the values found by our measurements. Of special interest is whether there is any significant dependence on the particle size.

4.4 The exponential parameter n as a function of the Cobalt content

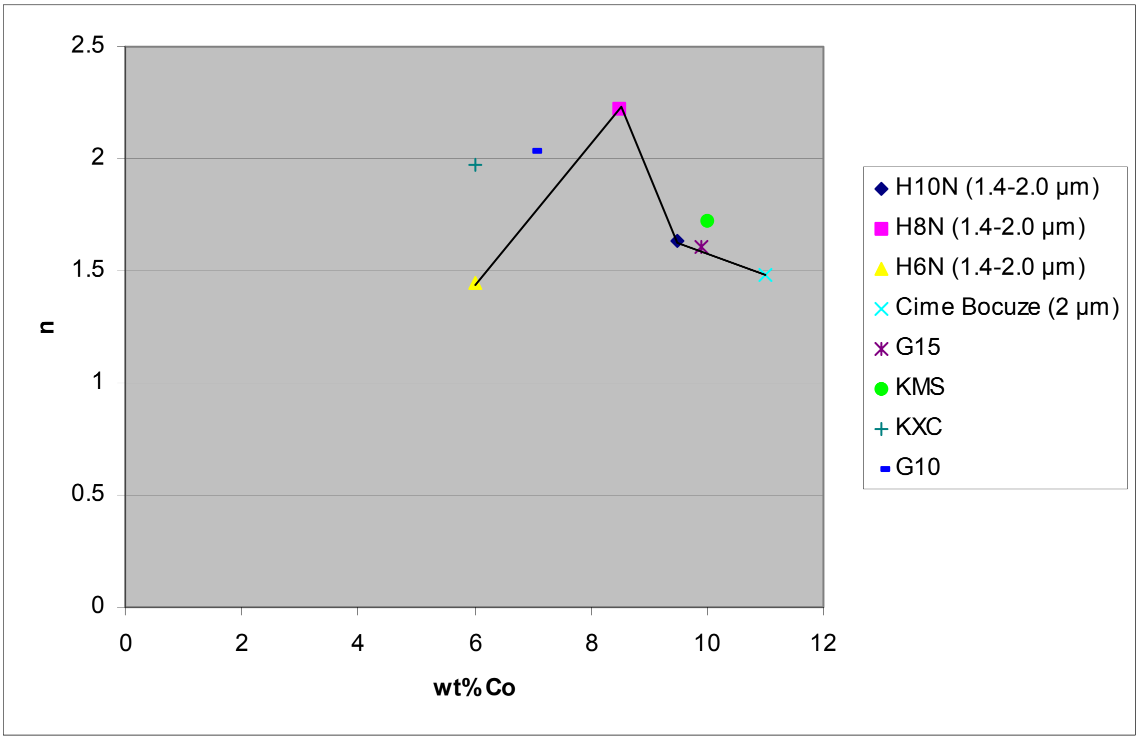

The n exponent is non dimensional. Again the relation to the particle size is of interest.

4.5 Compressive strength as a function of the Cobalt content for different particle sizes

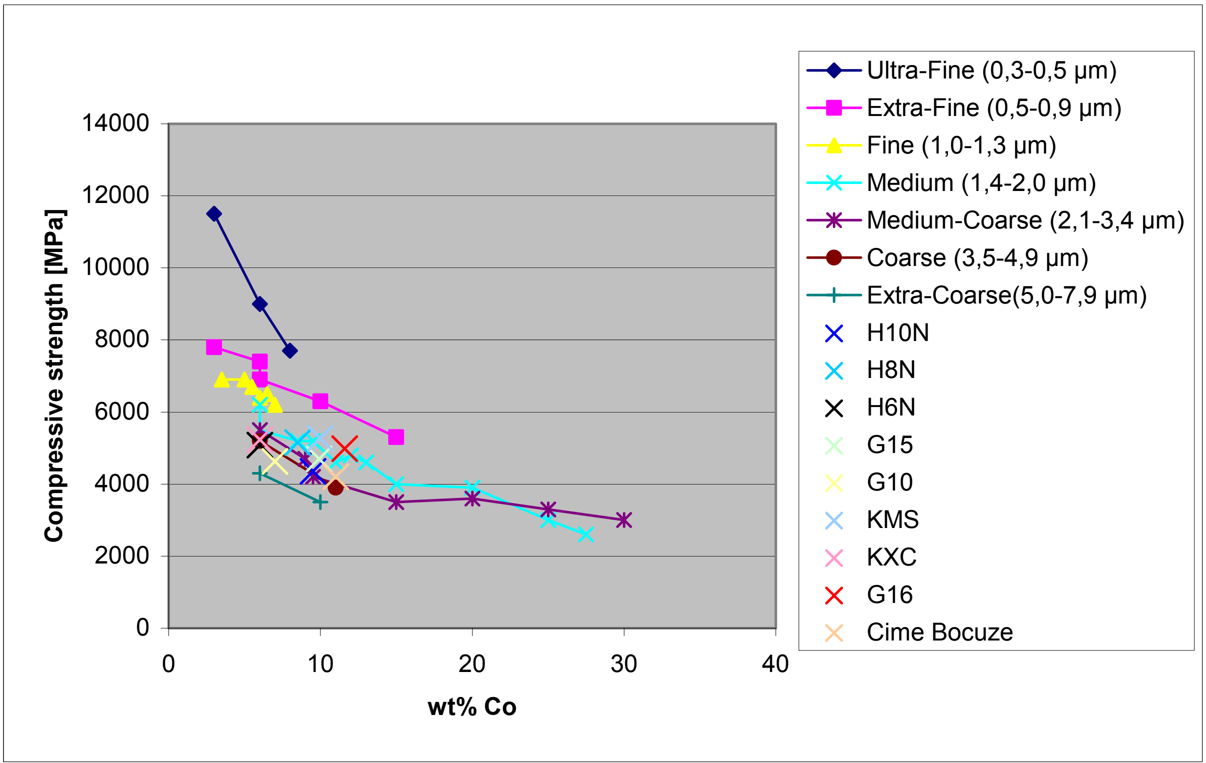

The compressive strength is increasing with decreasing particle size for a given Co content. This is expected since fracturing is most likely related to fracture surfaces initiated close to the particle surfaces. We observe that decreasing the particle size gives larger compressive strength for the same Co content. This is reasonable since smaller particles give more surfaces and probably larger strength for the same material. Thus this suggests that the bonding between the particles and the matrix is important for initiating the fracturing during compression. For a given particle size we expect that decreasing the Co content in the end gives lower strength (not shown in the figure above). The glue between the WC particles ultimately disappears when the Co disappears.

4.6 Hardness as a function of the Cobalt content for different particle sizes

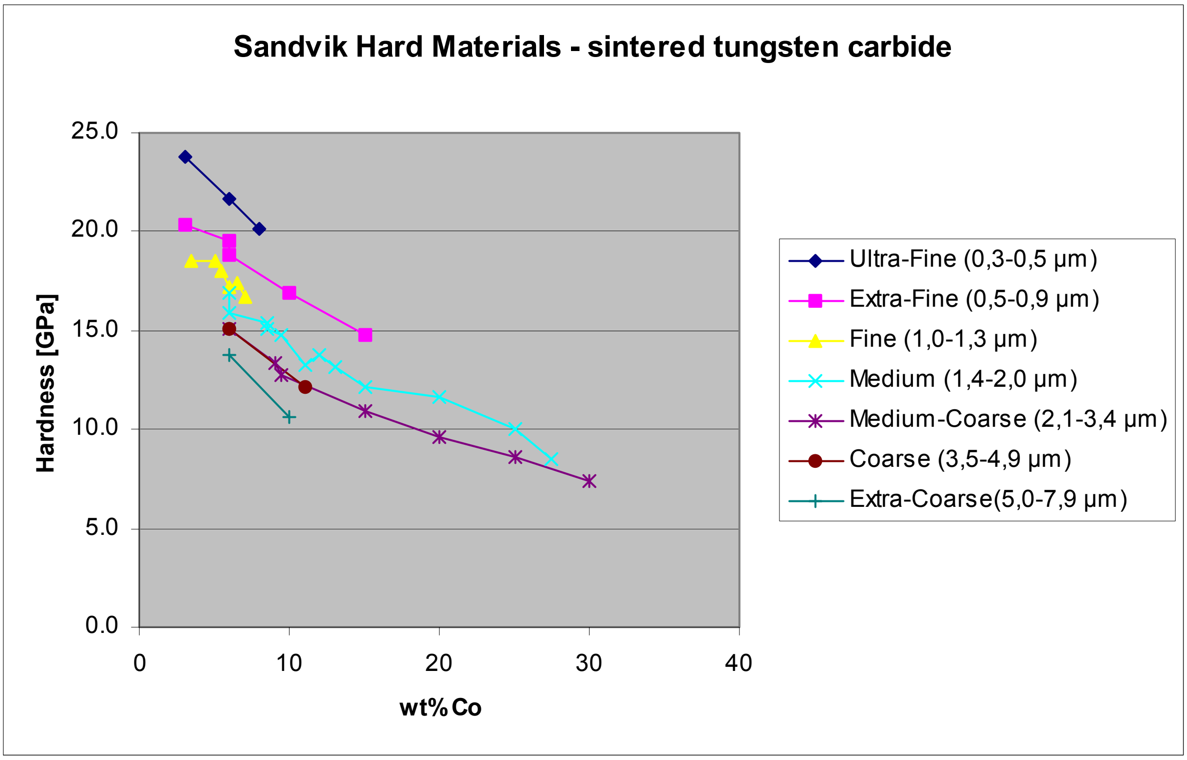

The hardness follows that same kind of relationship as the compressive strength. This is an important relation, which we will address later in this report.

4.7 Fracture strain during simple compression as a function of the Cobalt content for different particle sizes

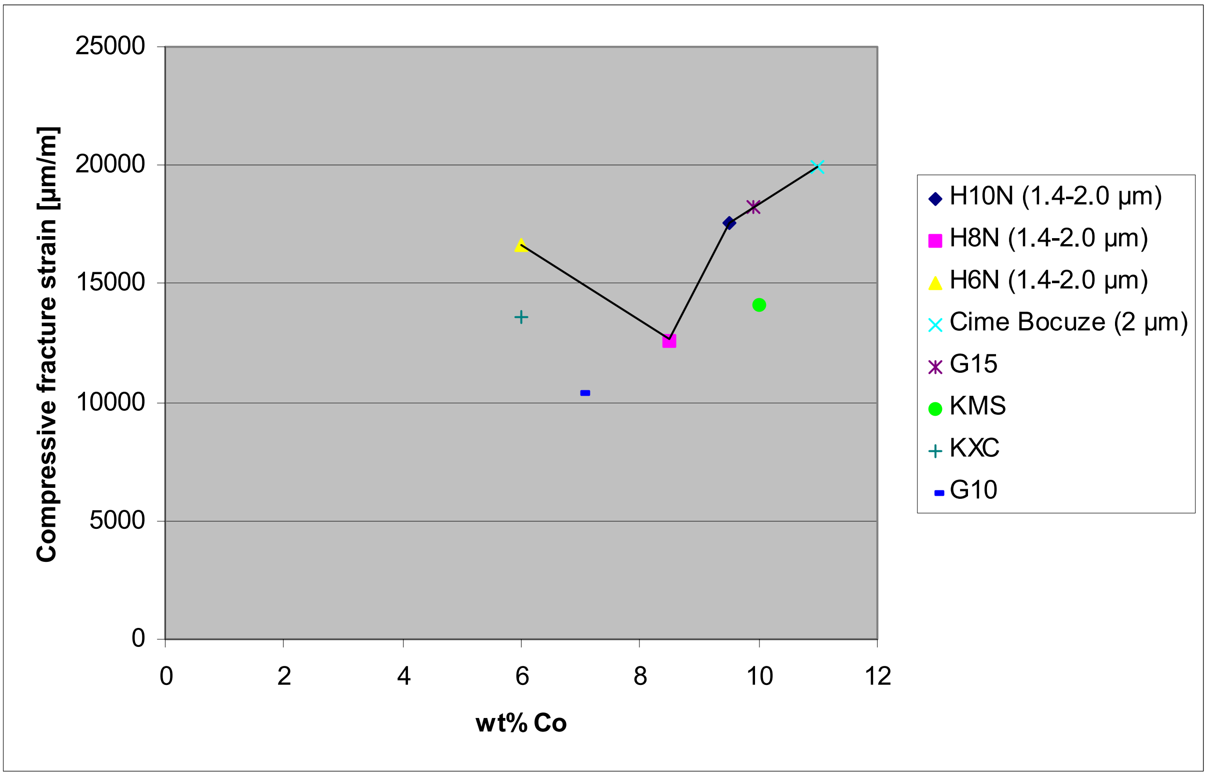

In general we expect that the fracture strain should increases with increasing Co content since the yield curve tends to be lower for increasing Co content. A simple hypothesis is that a given particle distribution corresponds to a given compressive strength, independent of the Co content of the material.

4.8 Estimated tensile fracture strain versus Cobalt content

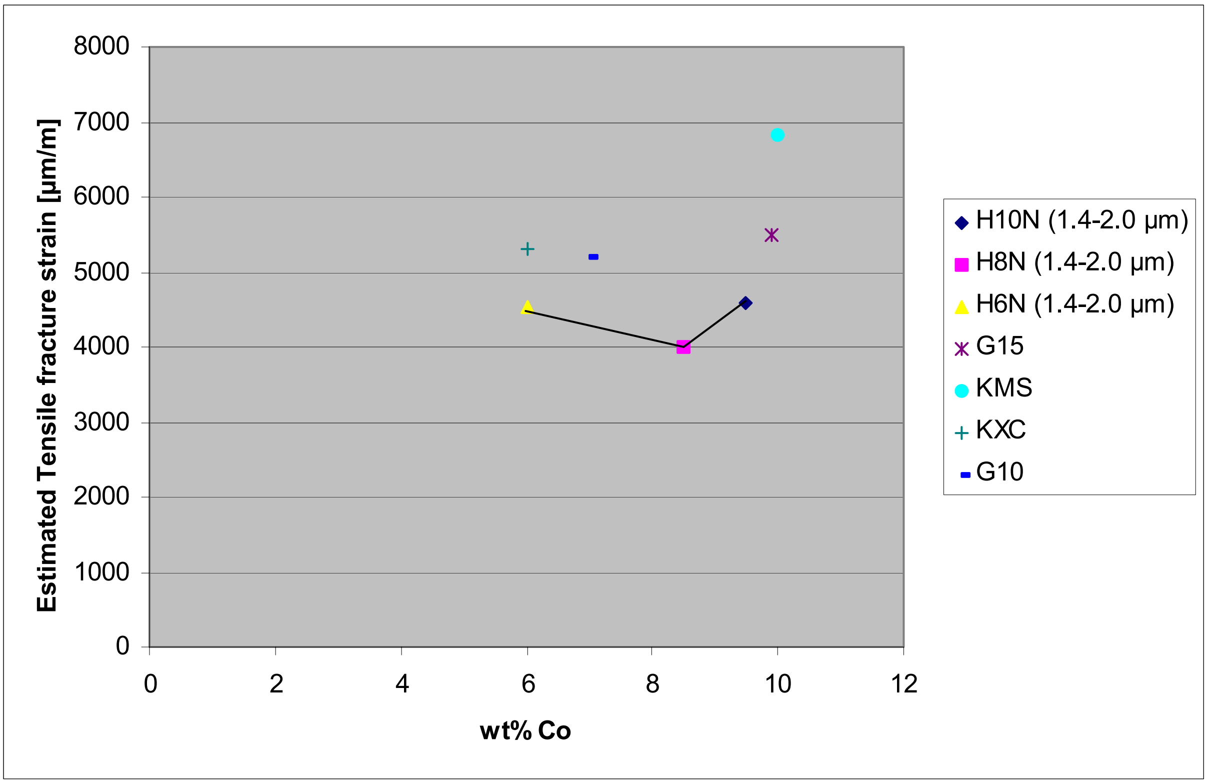

The tensile fracture strain was calculated by using the formula: $\varepsilon_{tf} = \frac{TRS}{E}\left(1 + a\left(\frac{TRS}{E}\right)^n\right)$,

where TRS is the transverse rupture strength reported in the literature. We expect that by increasing Co content the fracture strain should increase. This is not clearly seen in this picture, but is more clearly seen in the next figure. Only the first term is used to calculate the fracture strain in the next figure.

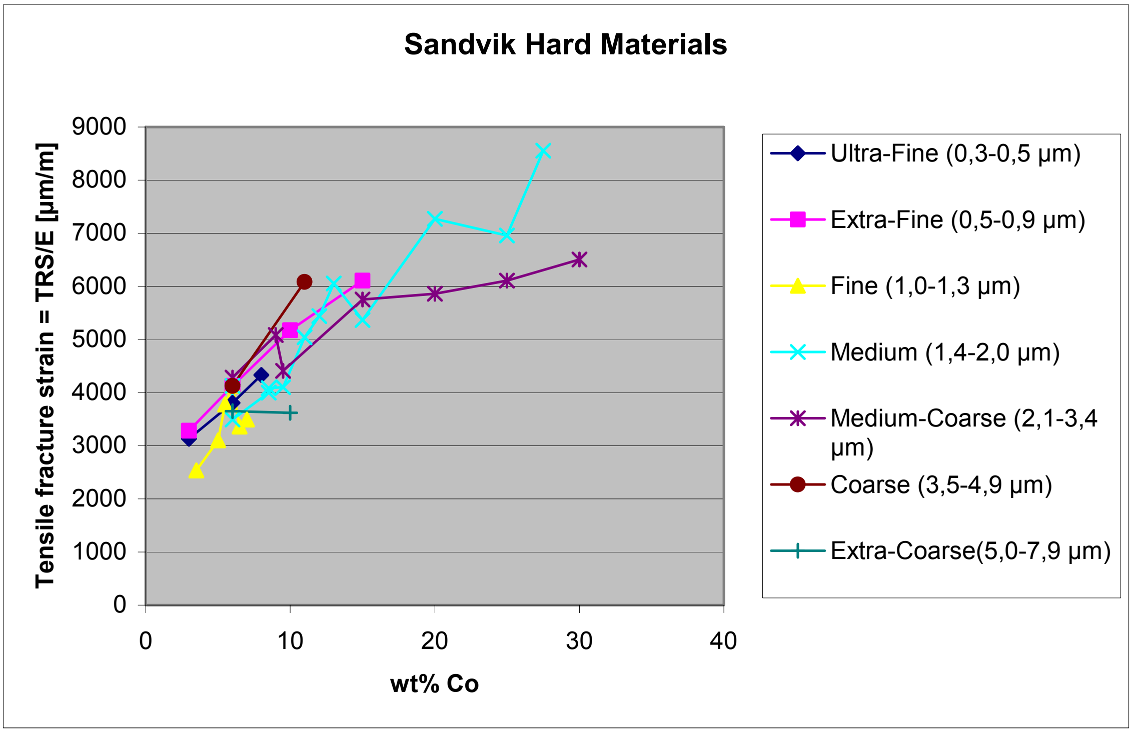

4.9 Transverse rupture strength as a function of Cobalt content for different particle sizes

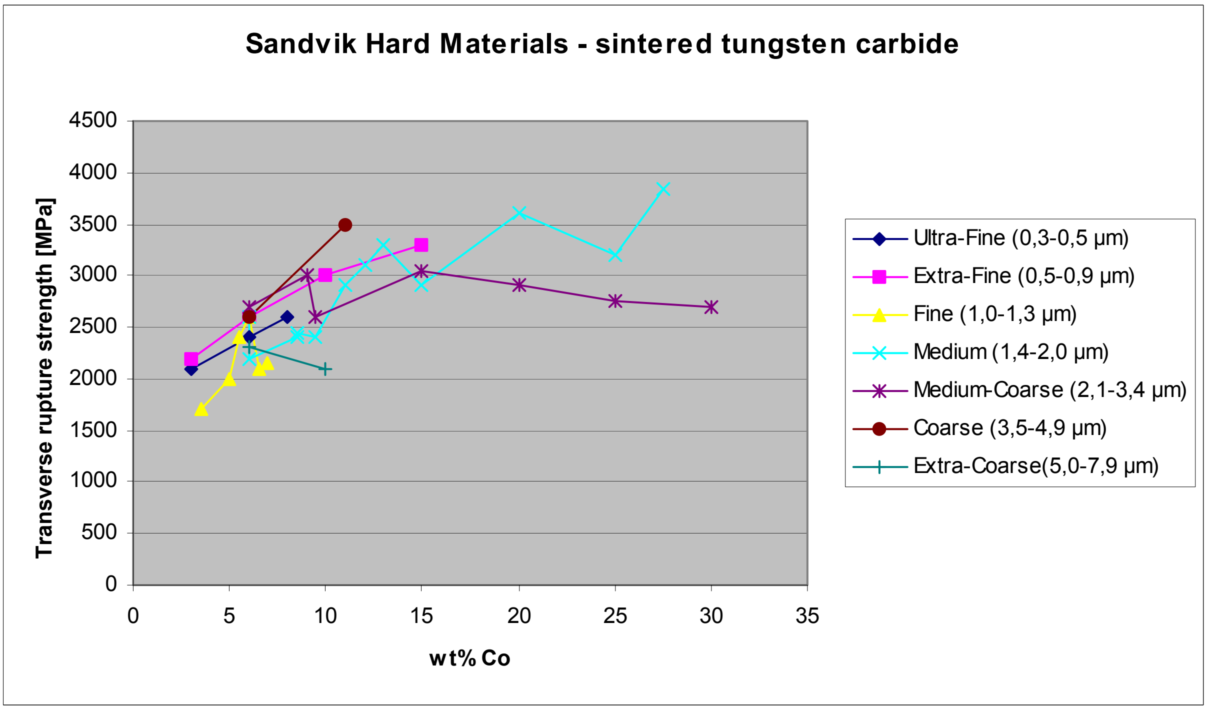

In general the fracture strength during tension increases with the Co content. The compressive strength decreased with the increased Co content. Why the transverse rupture strength shows the inverse relation ship is important. This suggests that fracturing during compression and during tension is related to different physical mechanisms on the particle level. Also the strength increases for smaller particles up to approximately 10 wt% Co.

4.10 Fracture toughness as a function of Cobalt content for different particle sizes

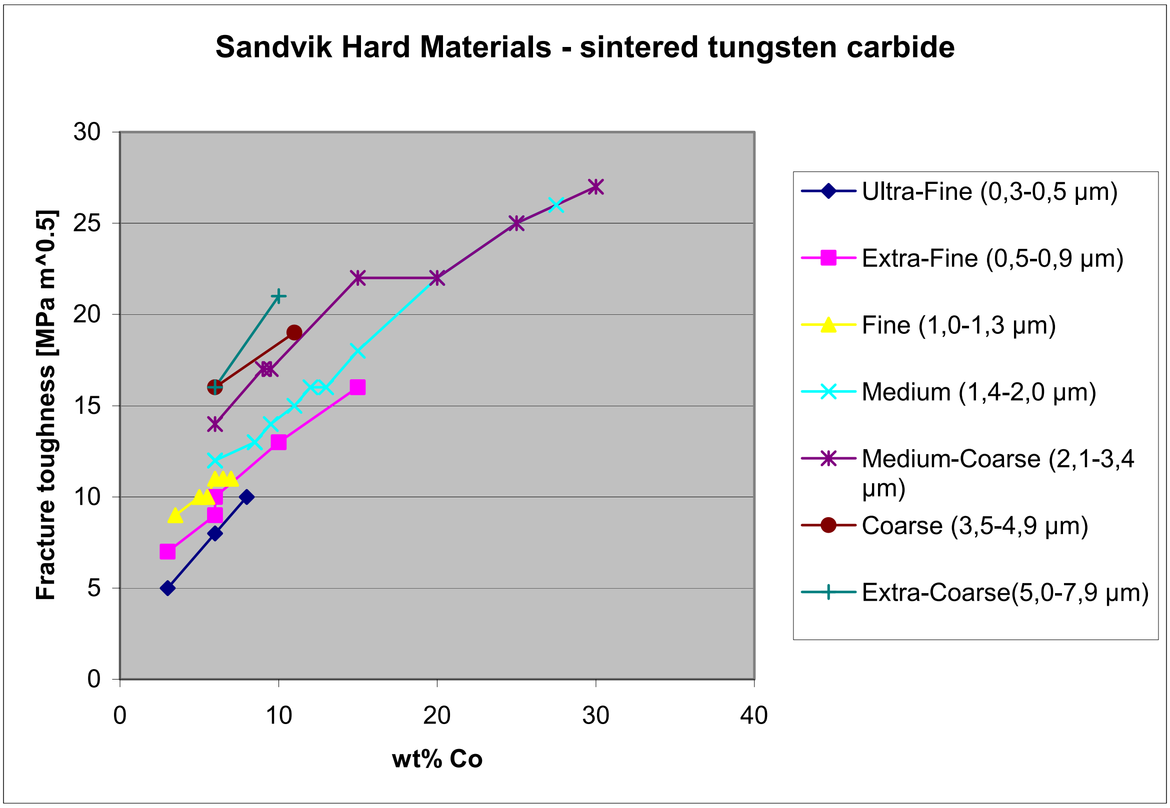

The fracture toughness is depending on the particle size.

4.11 Compressive strength versus hardness

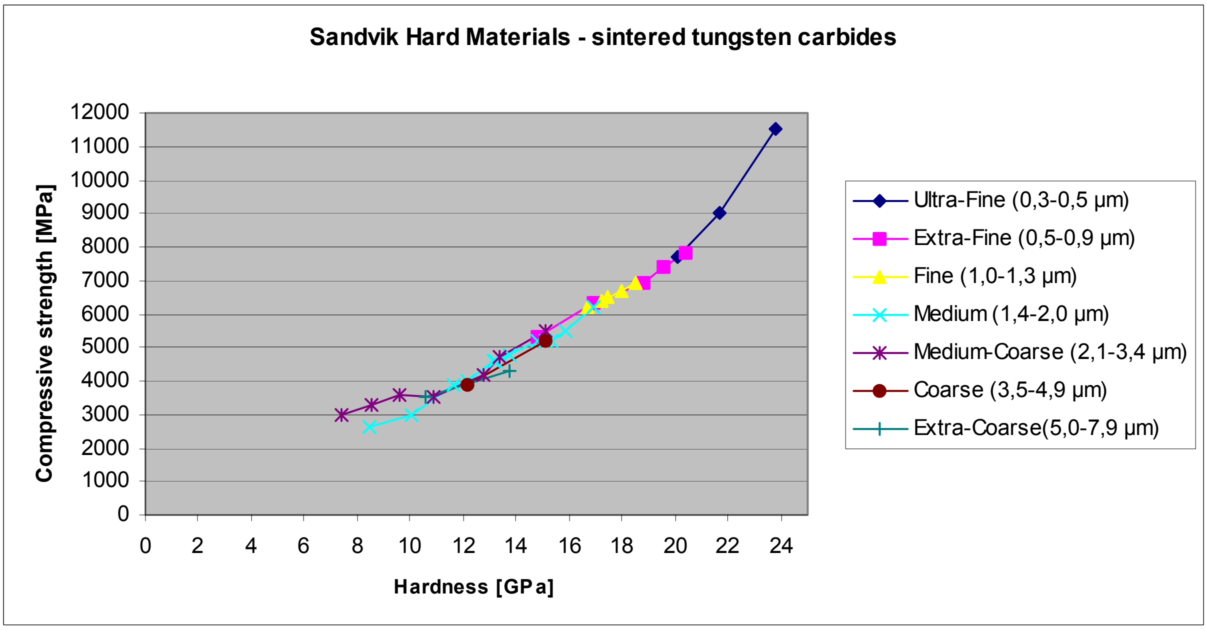

The compressive strength and the hardness follow a relationship that is not depending on the particle size. This suggests that hardness and compressive strength is related to the same physical mechanism.

4.12 Compressive strength versus transverse rupture strength

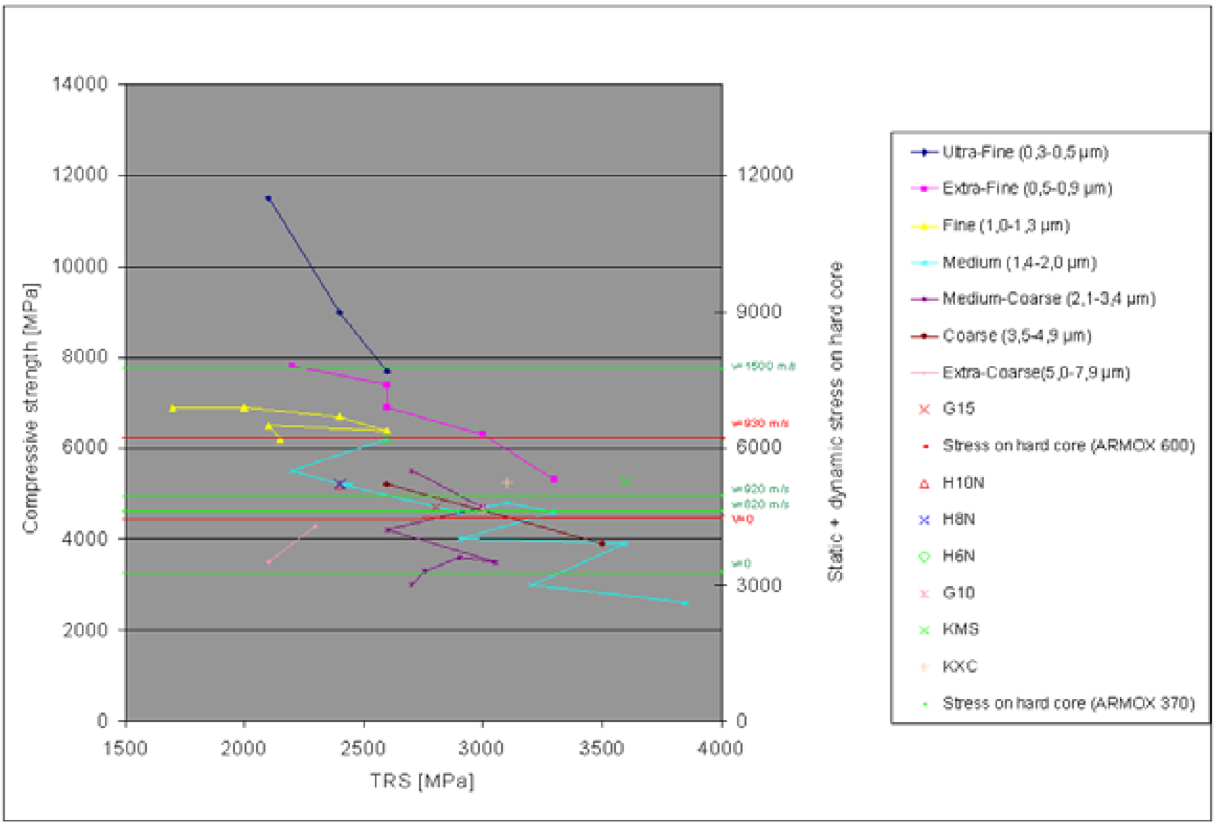

This figure is important for the overall conclusion for the hard core. The two lines with v=0 indicates the stress necessary for quasi-static penetration into two different steel plates. We observe that the strength of the G15 hard core is above the line for the standard steel Armox 370. Also 820 m/s impact is below the strength of the hardcore. When using 920 m/s the figure indicates that the hardcore should fracture. This is close to the experiments from the shooting range. With Armox 600 the hardcore G15 is able to penetrate quasi-statically. At 930 m/s the hardcore should fracture during penetration of Armox 600. This is also observed at the shooting range.

4.13 Compressive yield strain and stress versus Cobalt content

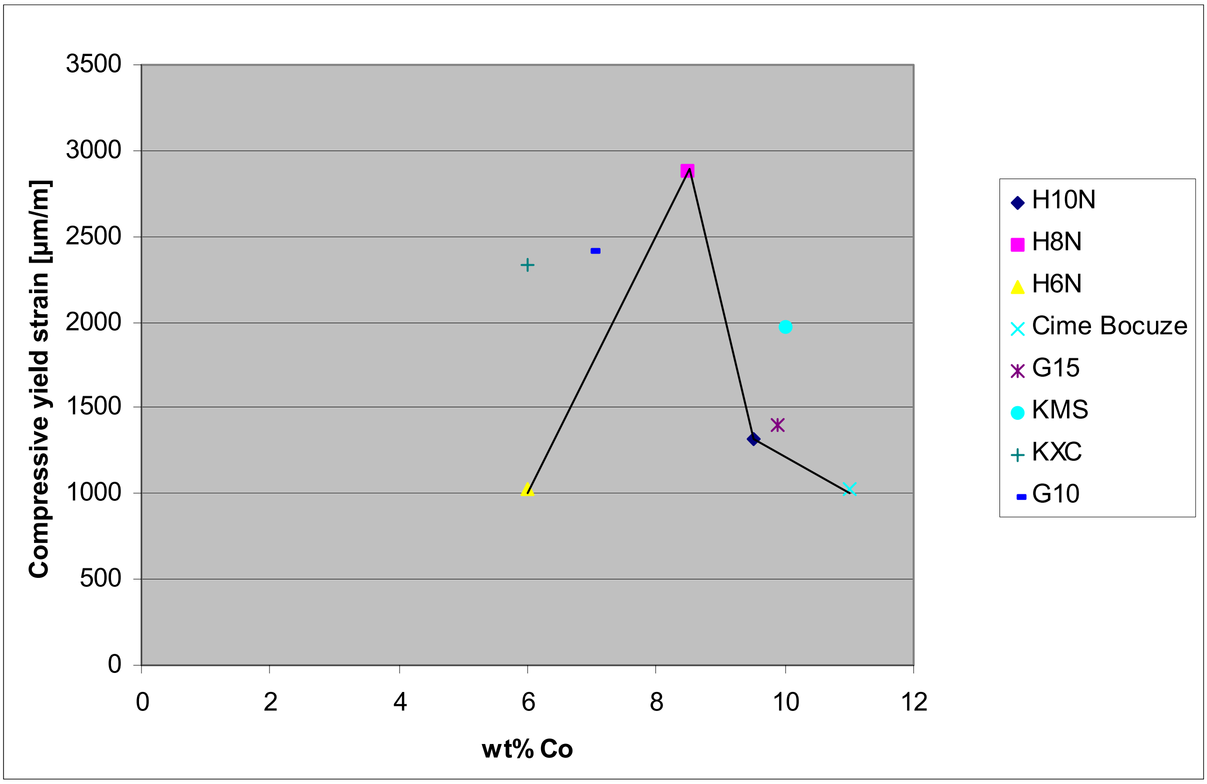

The compressive yield strain was calculated as shown in section 2.

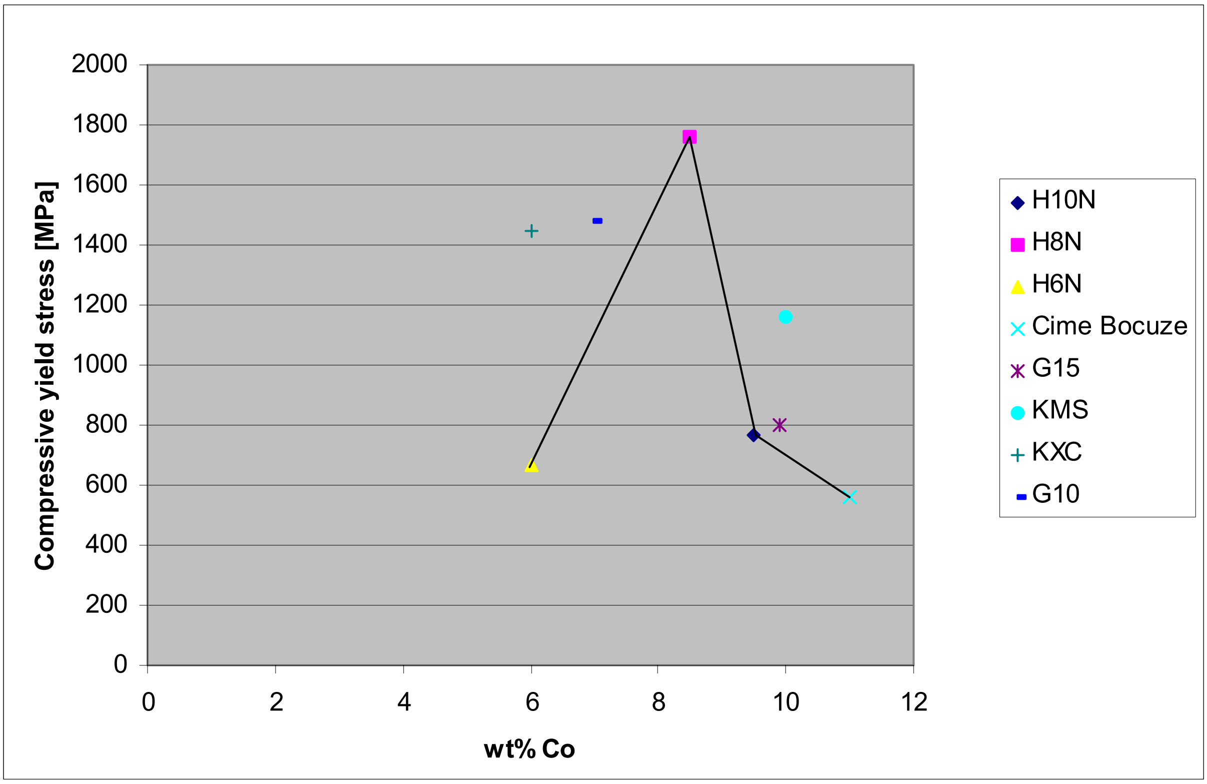

The compressive yield stress was calculated as shown in section 2.

4.14 The term $a\,\varepsilon^n$ as a function of Cobalt content for different strain values

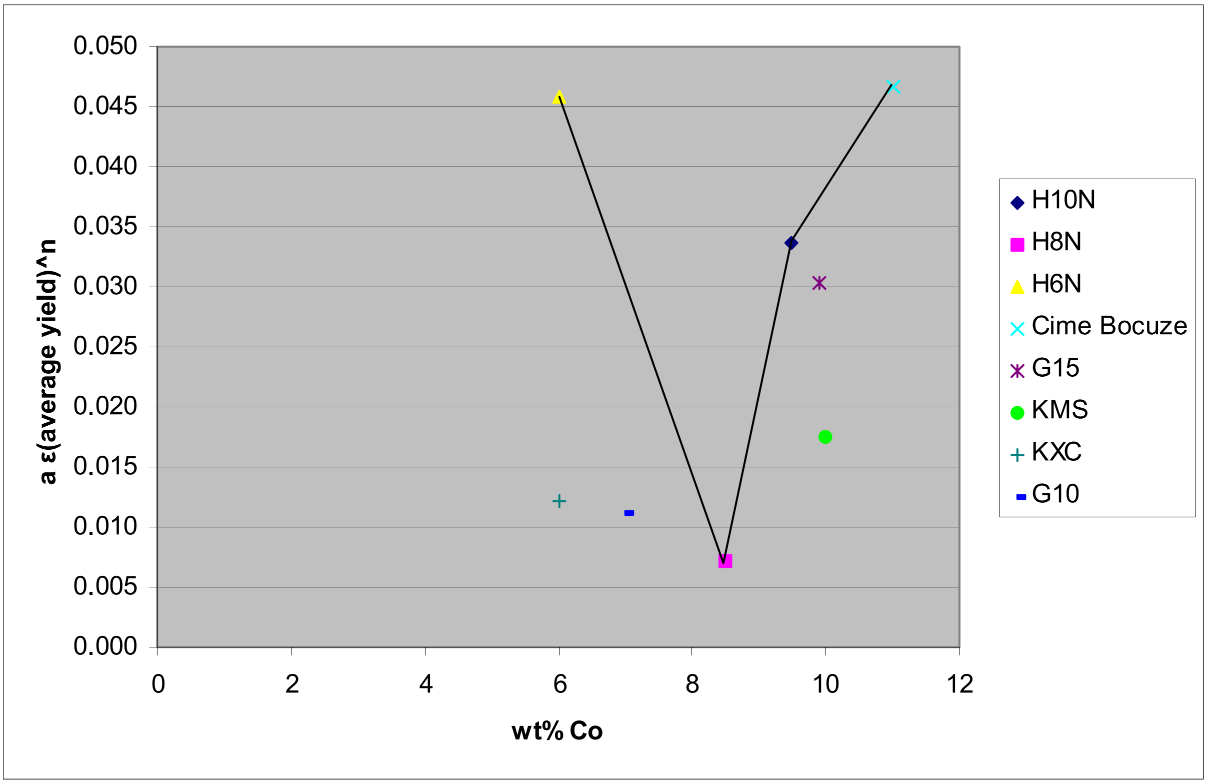

The term $a\,\varepsilon^n$ for the average yield strain, ε(average yield) = 1796 μm/m.

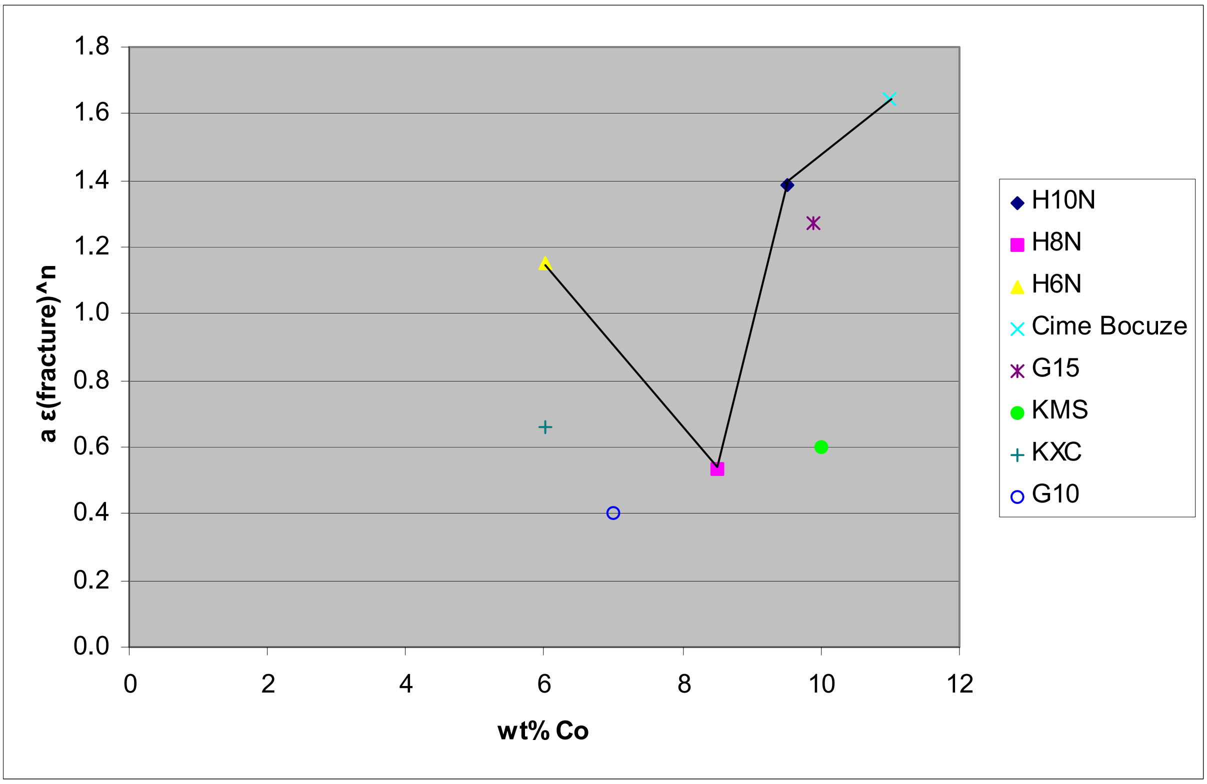

The term $a\,\varepsilon^n$ for the fracture strain, ε(fracture).

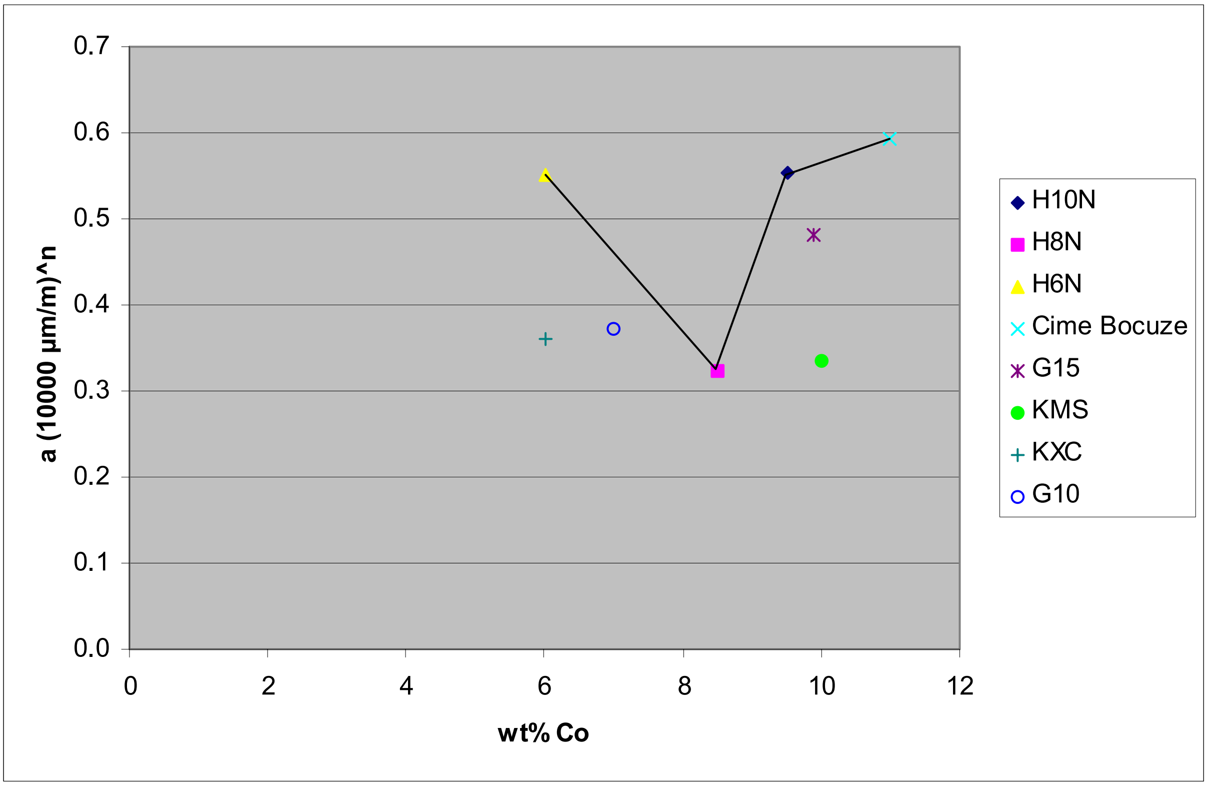

The term $a\ \varepsilon^n$ for the strain, ε = 10000 µm/m.

4.15 σ_{top} and ε_{top} as a function of Cobalt content

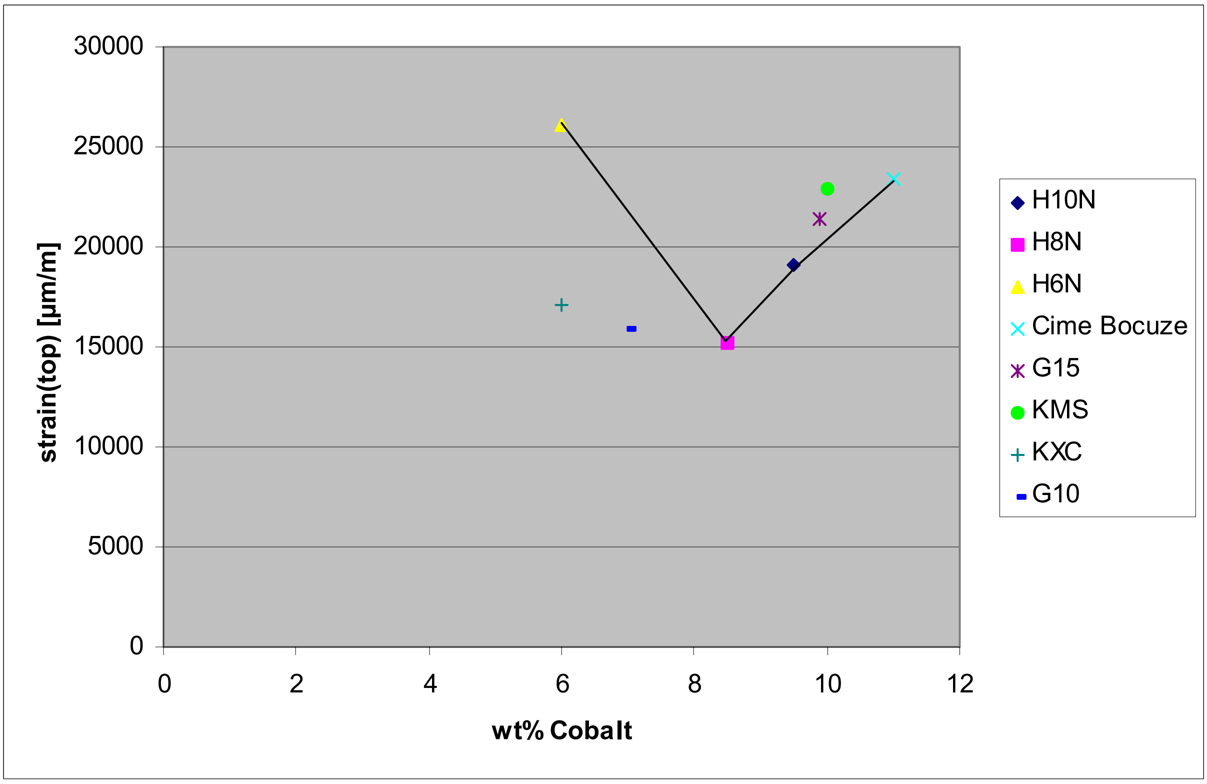

Strain(top), ε_{top}, is the strain when the function σ(ε) (Equation 2.1) reach the maximum value.

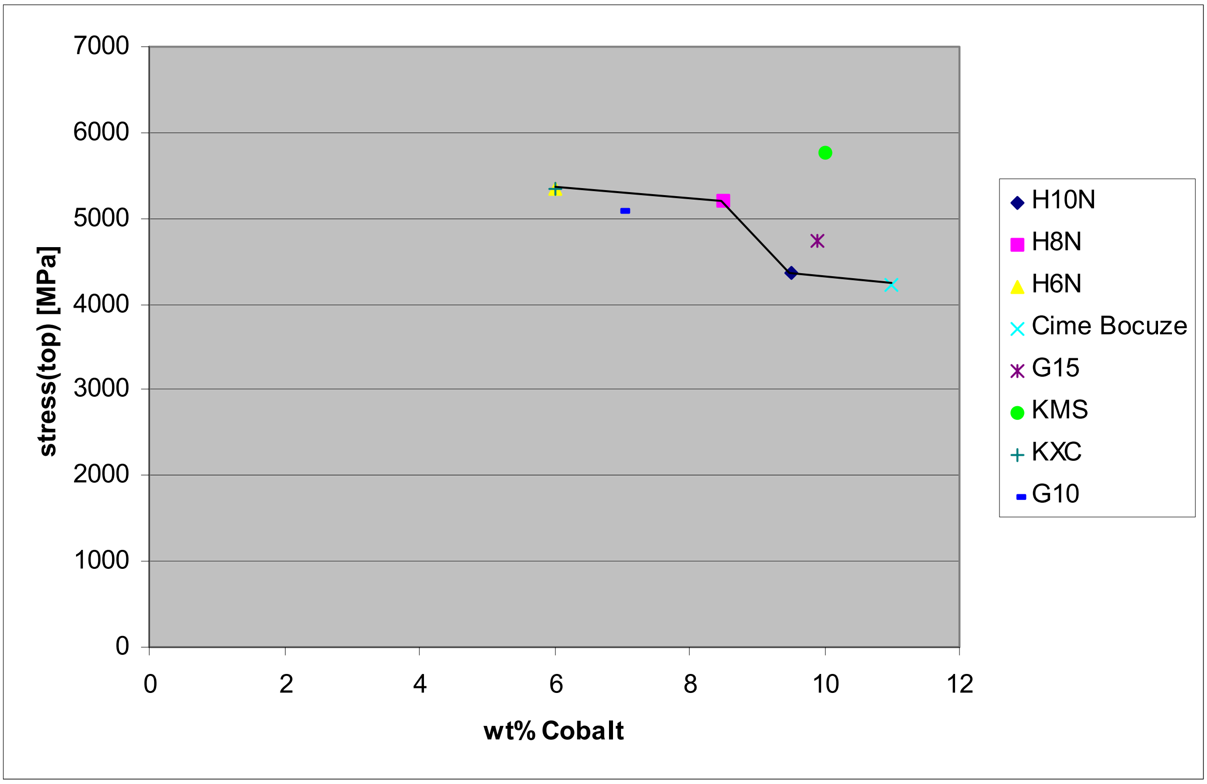

Stress(top), σ_{top}, is the stress when the function $\sigma(\varepsilon)$ (Equation 2.1) reach the maximum value.

5 CONCLUSION/DISCUSSION

We have examined and found material properties for different hard cores of sintered WC-Co penetrators. The overall conclusion is that the compressive strength of the hard core G15 is only marginally above the compressive strength necessary to penetrate Armox 370 at 860 m/s. By increasing the hardness of the target the penetration capability of the hardcore should decrease significantly to about a third of the original value. Changing the hardcore to a material with more compressive strength should in general increase the penetration capability of the hardcore significantly. We believe that the transverse rupture strength should be approximately the same as for the G15 hard core.

A APPENDIX

The following material parameters were used in the analytical theory:

Properties for sintered WC-Co hardmetals										
Product name	Poisson's ratio	Coercivity, H_c [Oersted]	Density [g/cm^3]	wt% Co	TRS [N/mm^2]	HV30 [GPa]	Compressive strength [GPa]	Young's Modulus [GPa]	Fracture toughness [MN/m$^{(3/2)}$]	Average grain size [μm]
G15	0.22	136	14.55	9.9	2800	13.4 – 14.1	4.5	580	14.2	
G10			14.85	7	3000	14.9 – 16.0				
KMS			14.4	10	3600	16.0 – 16.8				
KXC			14.9	6	3100	16.1 – 17.1				
G16			14.35	11.6	3000	12.7 – 13.6	4.95	579		
H10N	0.22		14.5	9.5	2400	14.8	5.2	585	14	1.4 - 2.0
H8N	0.22		14.65	8.5	2400	15.3	5.2	600	13	1.4 - 2.1
H6N	0.21		15	6	2600	16.9	6.2	630	11	1.4 - 2.2
Cime Bocuze			14.5	11		13.2				2
Baldonit										

Table A.1: Properties given by the manufacturers.

Note: The hardness HV30 is calculated in GPa by using the formulae:

$HV30[GPa]=HV30[kg/mm^2] \cdot 1.058 \cdot 10^{-3}$

DATA SHEET 2000-06-06

ARMOX™ 370T

(ARMOX 370S C 9640X0052, MIL-A-12560, ARMOX 816 MVEE 816, ARMOX 370 TL 2350-0000)

CHEMICAL COMPOSITION
(ladle analysis)

C max %	Si %	Mn max %	P max %	S max %	Cr max %	Ni max %	Mo max %	B max %
0,32	0,1 – 0,4	1,2	0,015	0,010	1,0[1]	1,8[1]	0,7	0,005

The steel is grain-refined.
[1] For plate thicknesses >100 mm Cr ≤ 1,5 and Ni ≤ 3,5

MECHANICAL PROPERTIES

	Plate thickn. mm	Hardness HBW	Charpy-V –40°C[1] 10x10 test specimen[2]	Yield strength Rp0,2 N/mm²	Tensile strength Rm N/mm²	Elongation A5%	A50%
Class 1	3 < 20	380–430	Min. 20 Joule	Min. 1000	1150–1350	Min. 10	Min. 12
	20 < 40	340–390	Min. 25 Joule	Min. 900	1050–1250	Min. 11	Min. 13
	40 – 80	300–350	Min. 30 Joule	Min. 850	950–1150	Min. 12	Min. 14
Class 2	3 – 150	280–330	Min. 40 Joule	Min. 800	900–1100	Min. 13	Min. 15

[1] Average of three tests. Transverse to rolling direction.
Single value min 70% of specified average.
[2] For plate thicknesses under 12 mm subsize Charpy V-specimens are used. The specified minimum value is then proportional to the specimens cross-section.

TESTING

Brinell hardness test	EN ISO 6506-1	Each heat treatment individual
Charpy impact test	EN 10 045-1	Each heat and thickness >4 mm
Tensile testing	EN 10 002-1	Each heat and thickness <60 mm
Ultrasonic testing	SEL 072/077 Cl. 3	Each plate in thickness 60–150 mm

DELIVERY CONDITION Quenched and tempered.

DIMENSIONS ARMOX 370T is supplied in plate thicknesses 3–150 mm. More detailed information on dimensions is provided in our General Information brochure.

TOLERANCES Dimensional tolerances according to EN 10 029 excluding thickness tolerances
– Thickness tolerances:

Plate thickness in mm	Standard Tolerances in mm	By special agreement Tolerances in mm		
< 13	–0,0 + 0,8	-0,2 +0,6	or	+/– 0,4
13 < 20	+ 1,0	-0,2 +0,8	or	0,5
20 < 40	+ 1,2	-0,2 +1,0	or	0,6
40 < 60	+ 1,6	-0,3 +1,3	or	0,8
60 < 80	+ 2,0	-0,3 +1,7	or	1,0
80 < 110	+ 2,4	-0,4 +2,0	or	1,2
110 – 150	+ 3,0	-0,5 +2,5	or	1,5

Other thickness tolerances by special agreement.
Dimensional tolerances for plate with mill edge according to special agreement.
Flatness tolerances according to class N or according to special agreement.

SURFACE CONDITION According to EN 10 163-2 Class B Subclass 3.

GENERAL TECHNICAL DELIVERY CONDITION According to EN 10 021 and EN 10 204. Unless otherwise agreed, inspection documents are issued in English with certificates of 3.1B type.

HEAT TREATMENT ARMOX 370T may not be heated above the temperature listed below if guaranteed hardness is to be maintained.

	Thicknesses range	Max heating temperature
Class 1	3 < 20 mm	400°C
	20 < 40 mm	500°C
	40 – 80 mm	550°C
Class 2	3 – 150 mm	600°C

For further information on machining, cutting and welding, please see special brochure or contact us.
Appropriate health and saftey precautions must be taken when welding, cutting, grinding or otherwise working on the product. Grinding, especially of primer coated plates, may produce dust with high particle concentration. Our Technical Customer Service Department will provide further information on request.

SSAB OXELÖSUND

SSAB Oxelösund AB
S-613 80 Oxelösund
Phone. +46 155-25 40 00
Fax +46 155-25 40 73
Telex 50950 SSAB S

DATA SHEET

2000-06-06

ARMOX™ 600T

(ARMOX 600S)

CHEMICAL COMPOSITION (ladle analysis)

C max %	Si %	Mn max %	P max %	S max %	Cr max %	Ni max %	Mo max %	B max %
0,47	0,1 – 0,7	1,0	0,010	0,005	1,5	3,0	0,7	0,005

The steel is grain-refined.

MECHANICAL PROPERTIES

Hardness HBW	Charpy-V –40°C[1] 10x10 test specimen[2]	Yield strength[3] Rp 0,2 N/mm²	Tensile strength[3] Rm N/mm²	Elongation[3] A5%
570–640	Min. 12 Joule	Typical 1500	Typical 2000	Typical 7

[1] Average of three tests. Transverse to rolling direction. Single value min 70% of specified average.
[2] For plate thicknesses under 12 mm subsize Charpy V-specimens are used. The specified minimum value is then proportional to the specimens cross-section.
[3] The value will not be reported on the Test Certificate

TESTING

Brinell hardness test	EN ISO 6506-1	Each heat treatment individual
Charpy impact test	EN 10 045-1	Each heat and thickness
Tensile testing	–	Not tested on a regular basis.
Ultrasonic testing	SEL 072/77 CL. 3	Each plate in thickness 60–100 mm

DELIVERY CONDITION

Quenched and tempered.

DIMENSIONS

ARMOX 600T is supplied in plate thicknesses 5–100 mm. Plate thicknesses ≥ 25 mm are supplied with mill edge or by special agreement only.

TOLERANCES

Dimensional tolerances according to EN 10 029 excluding thickness tolerances
– Thickness tolerances:

Plate thickness in mm	Standard Tolerances in mm	
< 13	-0,0	+ 0,6
13 < 20		+ 0,8
20 < 40		+ 1,0
40 < 60		+ 1,4
60 < 80		+ 1,6
80 - 100		+ 2,0

Other thickness tolerances by special agreement.
Dimensional tolerances for plate with mill edge according to special agreement.
Flatness tolerances according to class N or according to special agreement.

SURFACE CONDITION

According to EN 10 163-2 Class B Subclass 3.

GENERAL TECHNICAL DELIVERY CONDITION

According to EN 10 021 and EN 10 204. Unless otherwise agreed, inspection documents are issued in English with certificates of 3.1B type.

HEAT TREATMENT AND FABRICATION

ARMOX 600T may not be heated above 180°C (360°F) if guaranteed hardness is to be maintained.

For further information on machining, cutting and welding, please see special brochure or contact us.

Appropriate health and saftey precautions must be taken when welding, cutting, grinding or otherwise working on the product. Grinding, especially of primer coated plates, may produce dust with high particle concentration. Our Technical Customer Service Department will provide further information on request.

SSAB OXELÖSUND

SSAB Oxelösund AB S-613 80 Oxelösund | Phone. +46 155-25 40 00 | Fax +46 155-25 40 73 | Telex 50950 SSAB S

The figures below are showing the function $\sigma(e) = \frac{3Ge}{1+a'e^{n'}}$ fitted to table values of this function made in Mathematica version 4.0.1.0.

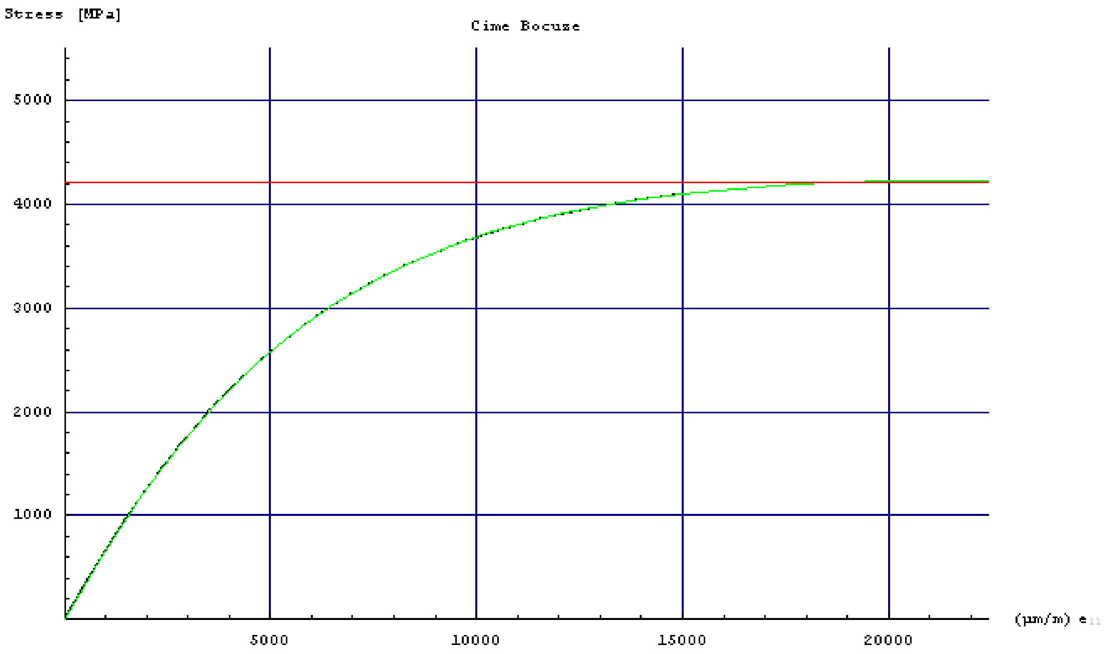

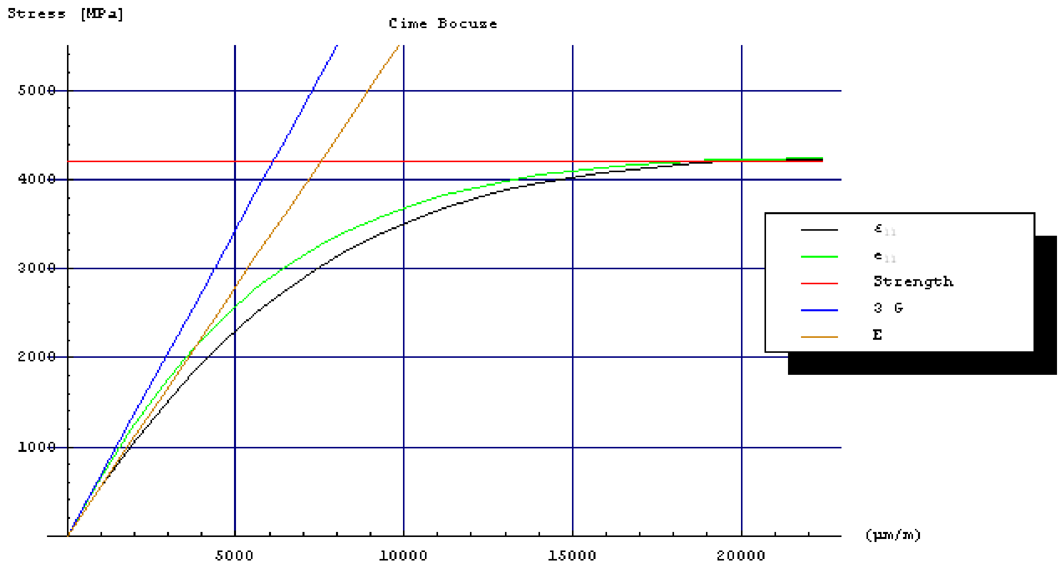

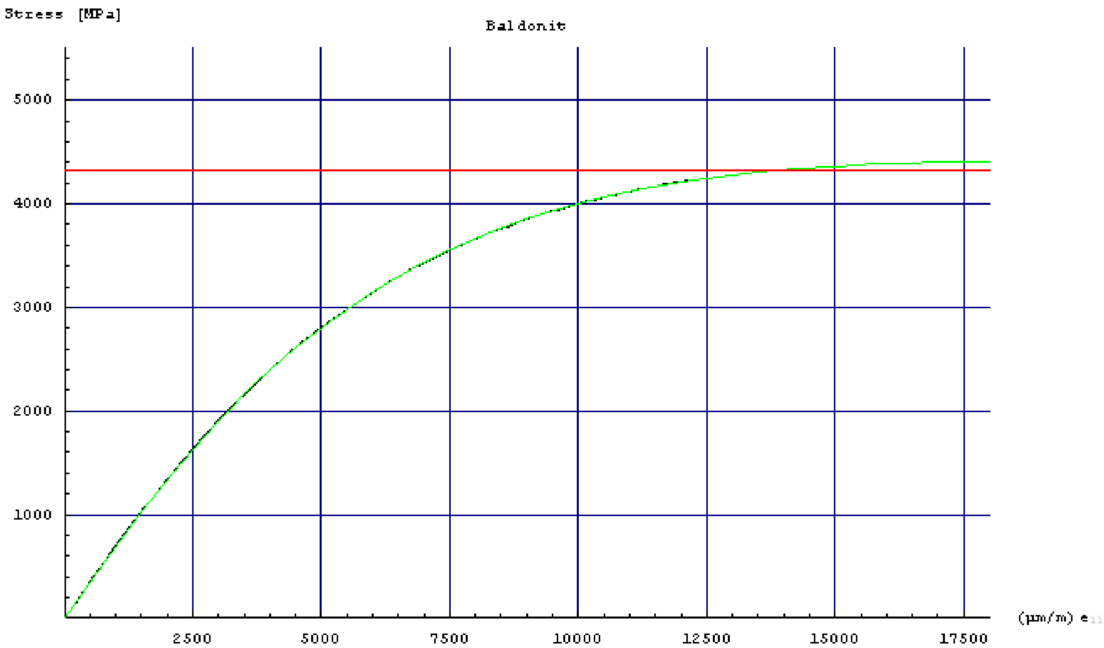
Stress [MPa]
Baldonit
5000
4000
3000
2000
1000
2500
5000
7500
10000
12500
15000
17500
(µm/m) e11

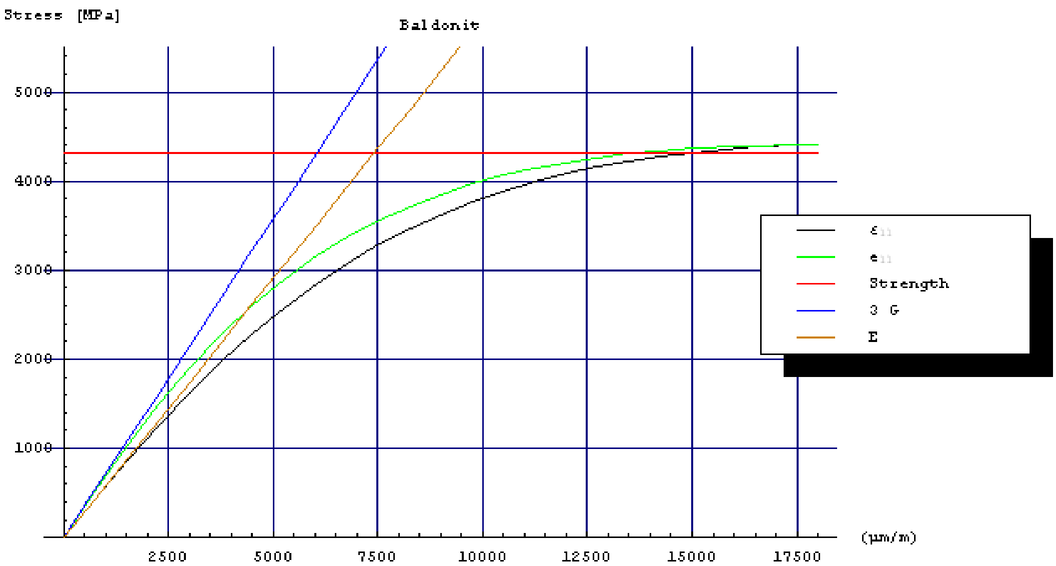
Stress [MPa]
Baldonit
5000
4000
3000
2000
1000
2500
5000
7500
10000
12500
15000
17500
(µm/m)
ε11
e11
Strength
3 G
E

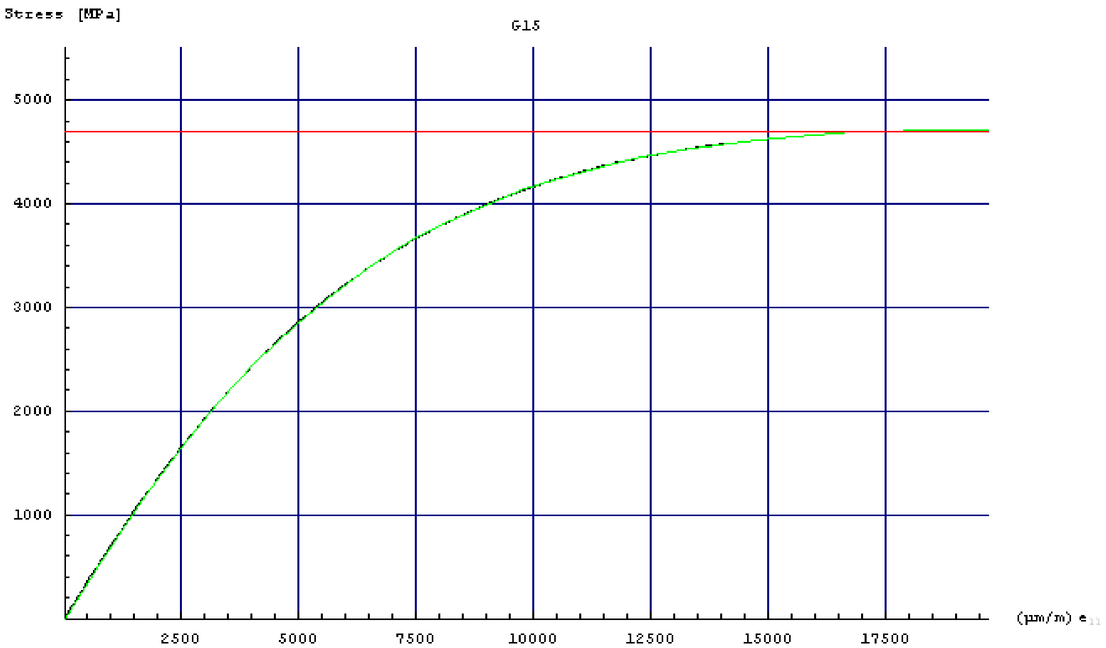
Stress [MPa]
G15
5000
4000
3000
2000
1000
2500
5000
7500
10000
12500
15000
17500
(μm/m) e11

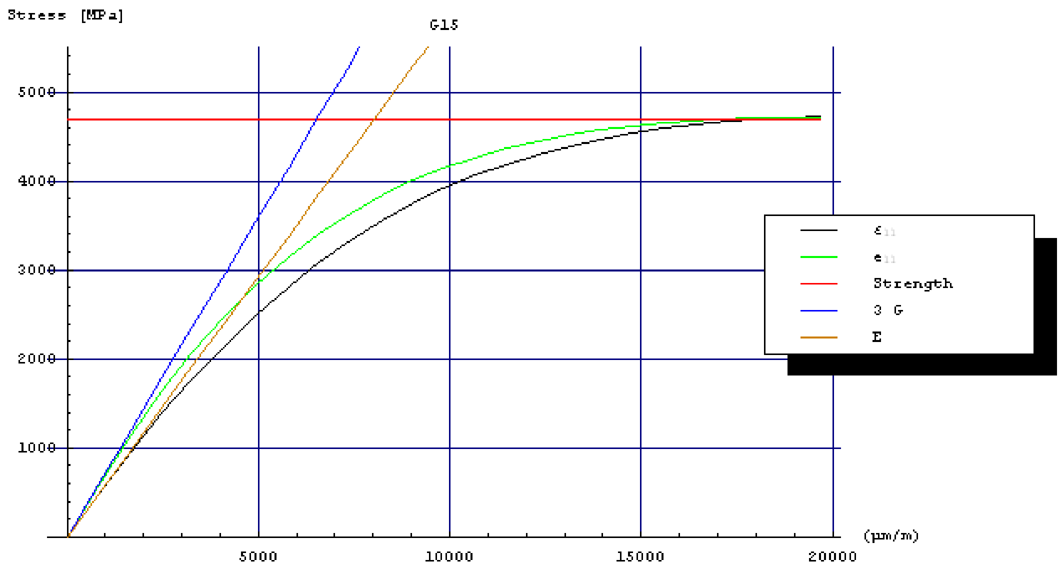
Stress [MPa]
G15
5000
4000
3000
2000
1000
5000
10000
15000
20000
(μm/m)
ε11
e11
Strength
3 G
E

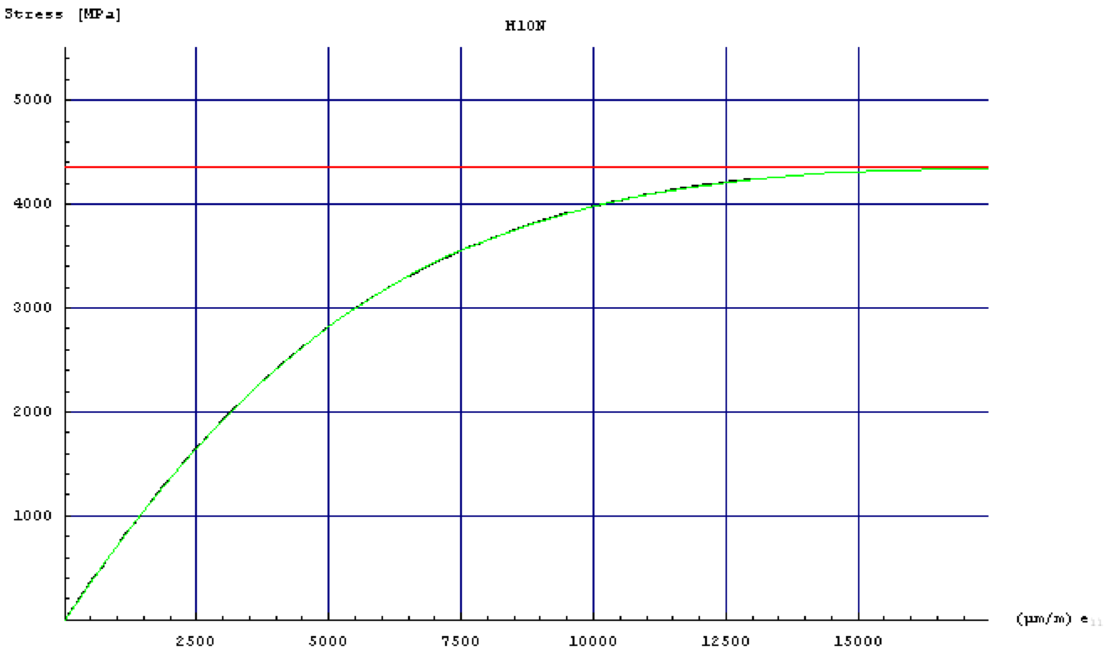
Stress [MPa]
H10N
5000
4000
3000
2000
1000
2500
5000
7500
10000
12500
15000
(μm/m) e11

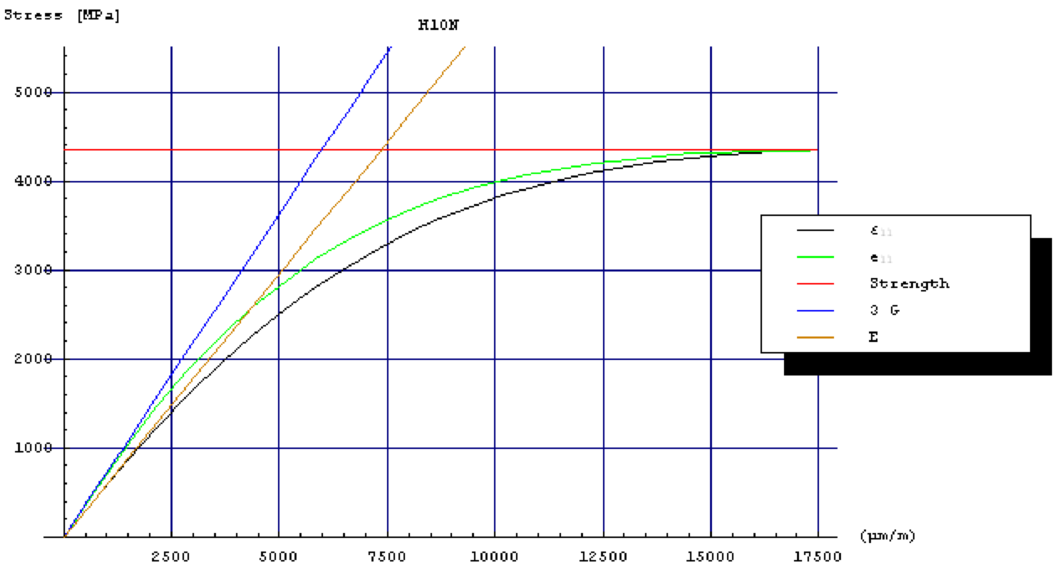
Stress [MPa]
H10N
5000
4000
3000
2000
1000
2500
5000
7500
10000
12500
15000
17500
(μm/m)
ε11
e11
Strength
3 G
E

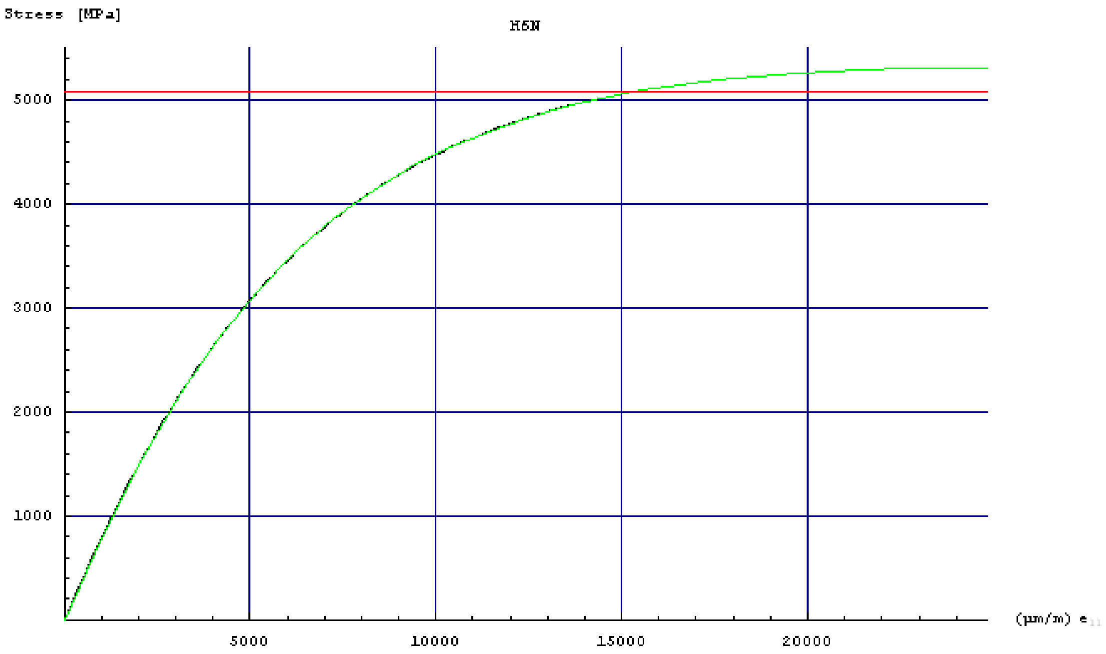
Stress [MPa]
H6N
5000
4000
3000
2000
1000
5000
10000
15000
20000
(µm/m) e11

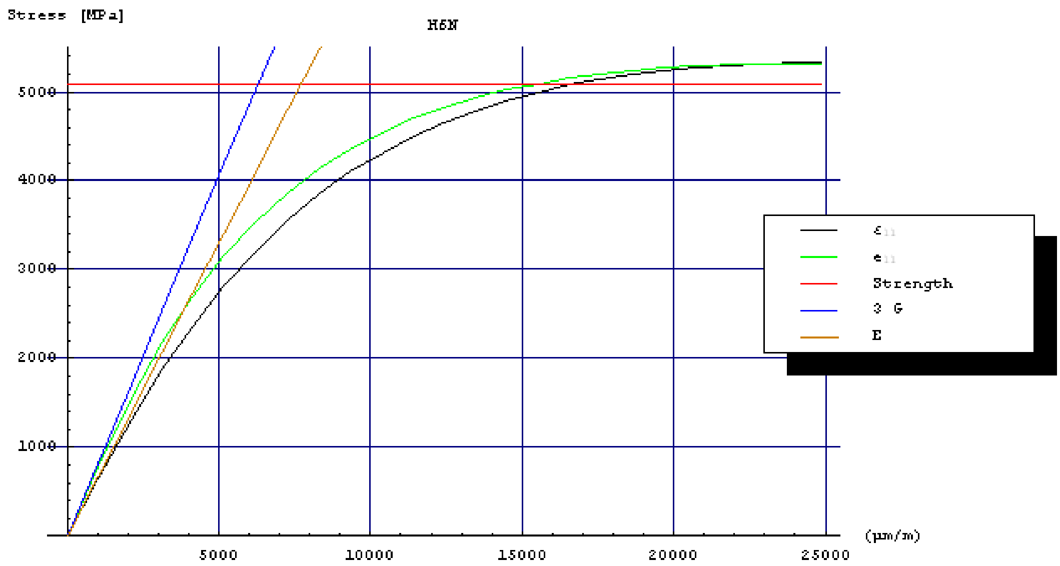
Stress [MPa]
H6N
5000
4000
3000
2000
1000
5000
10000
15000
20000
25000
(µm/m)
ε11
e11
Strength
3 G
E

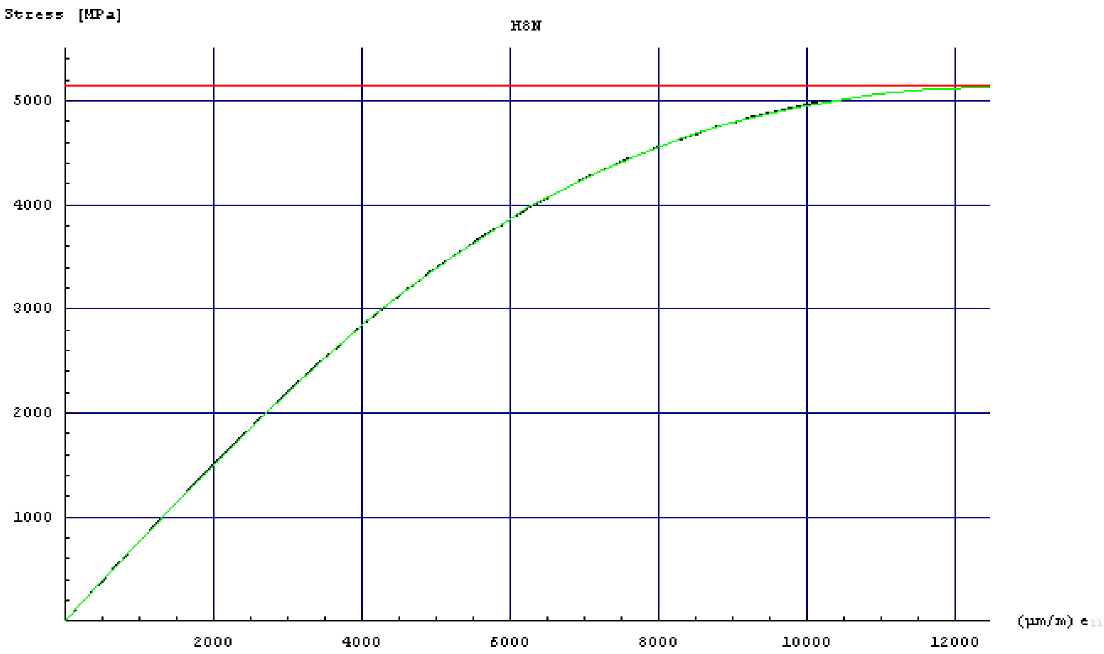
Stress [MPa]
H8N
5000
4000
3000
2000
1000
2000
4000
6000
8000
10000
12000
(μm/m) e11

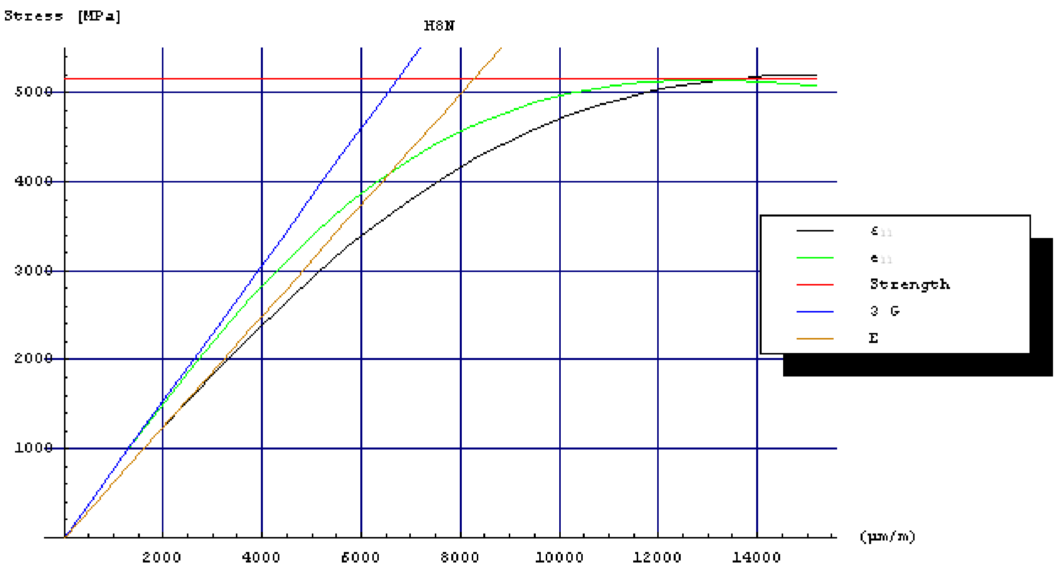
Stress [MPa]
H8N
5000
4000
3000
2000
1000
2000
4000
6000
8000
10000
12000
14000
(μm/m)
ε11
e11
Strength
3 G
E

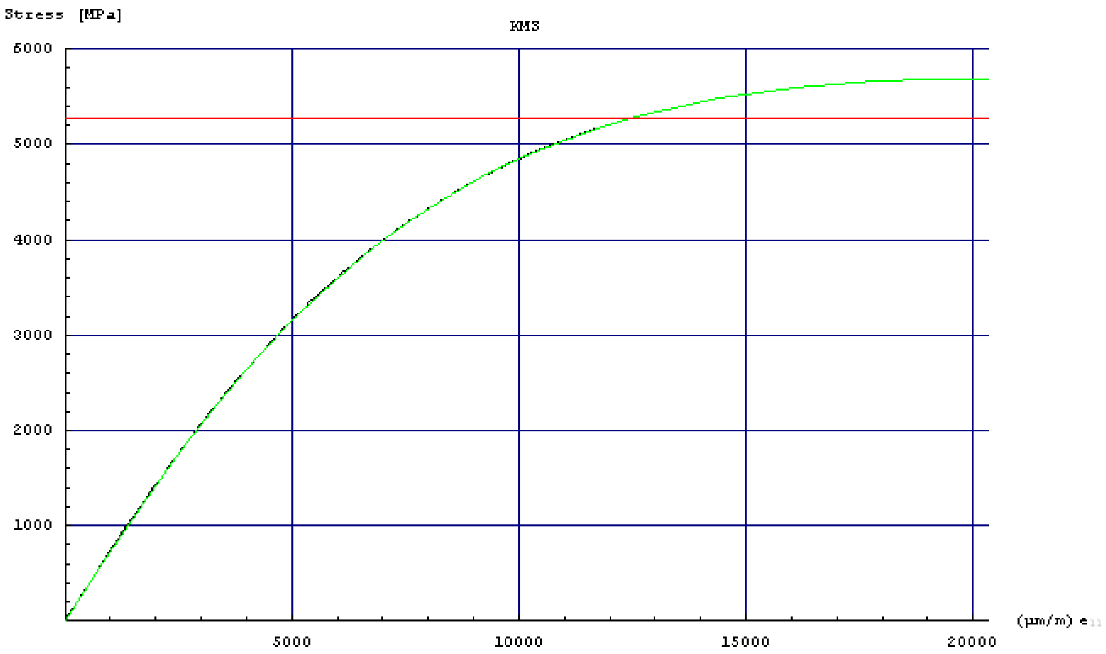
Stress [MPa]
KMS
6000
5000
4000
3000
2000
1000
5000
10000
15000
20000
(µm/m) e11

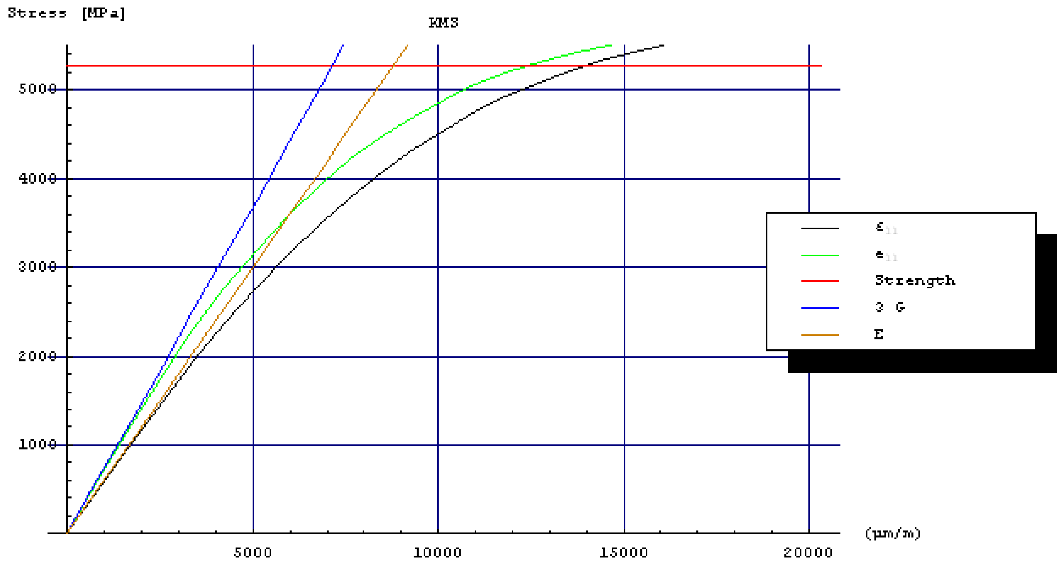
Stress [MPa]
KMS
5000
4000
3000
2000
1000
5000
10000
15000
20000
(µm/m)
ε11
e11
Strength
3 G
E

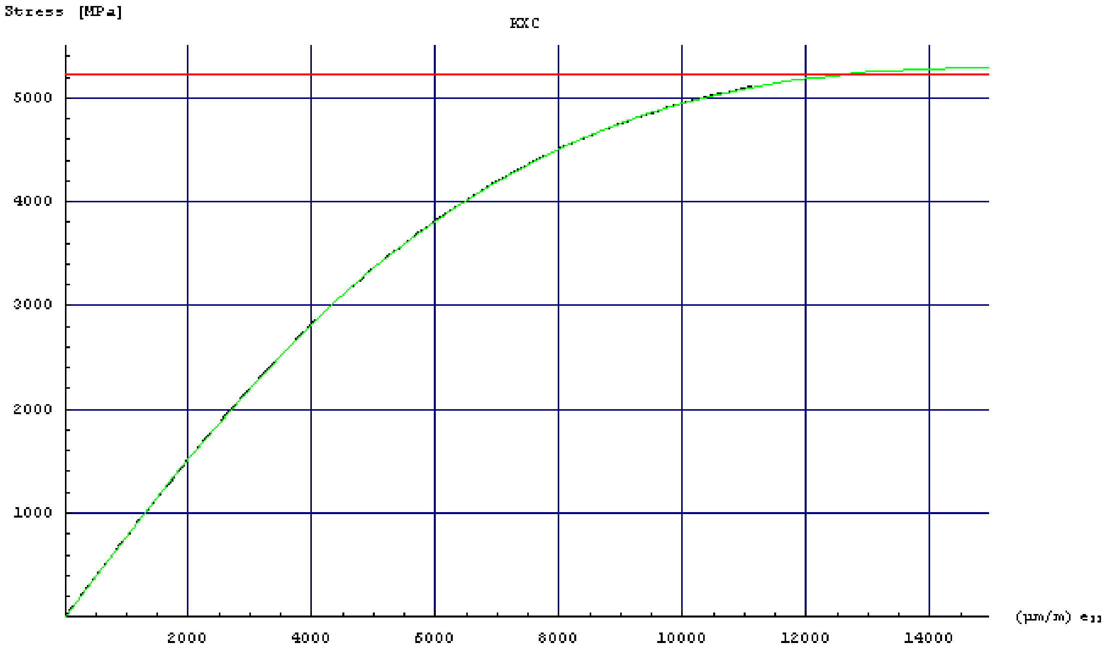
Stress [MPa]
KXC
5000
4000
3000
2000
1000
2000
4000
6000
8000
10000
12000
14000
(μm/m) e₁₁

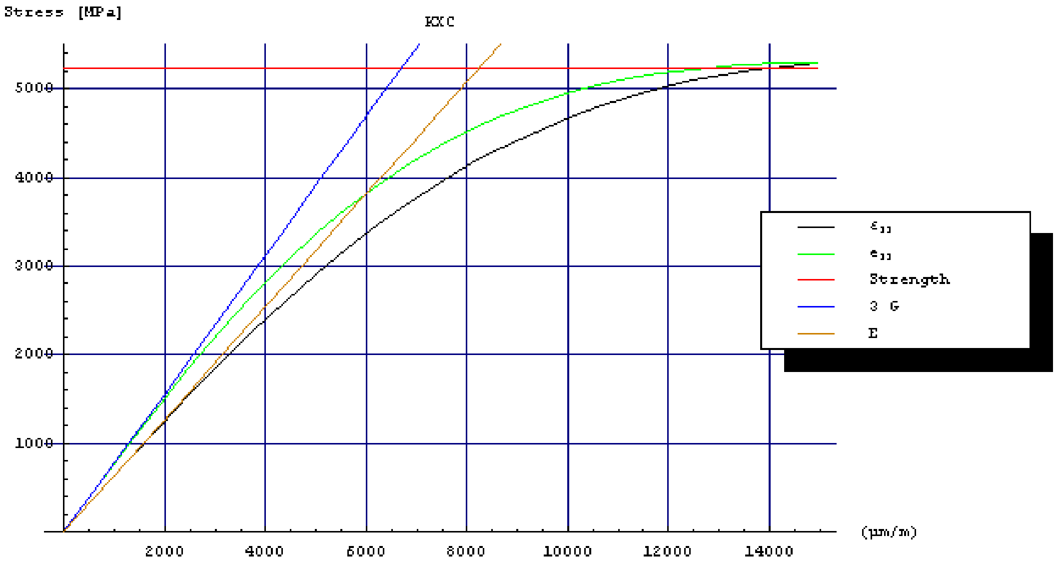
Stress [MPa]
KXC
5000
4000
3000
2000
1000
2000
4000
6000
8000
10000
12000
14000
(μm/m)
ε₁₁
e₁₁
Strength
3 G
E

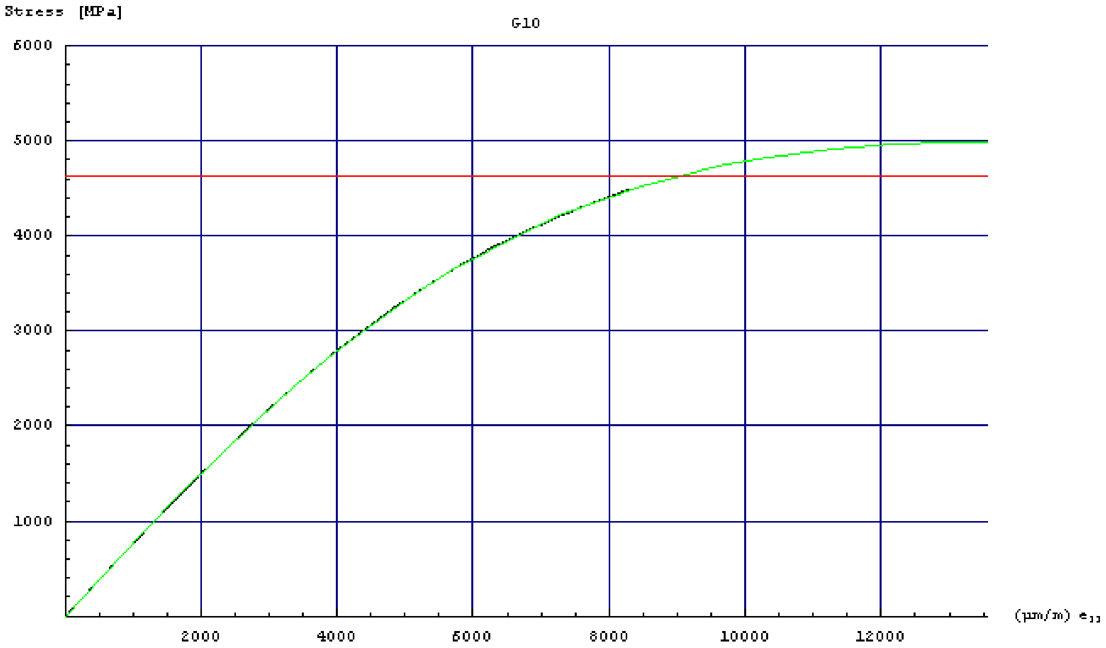
Stress [MPa]
G10
6000
5000
4000
3000
2000
1000
2000
4000
6000
8000
10000
12000
(μm/m) e11

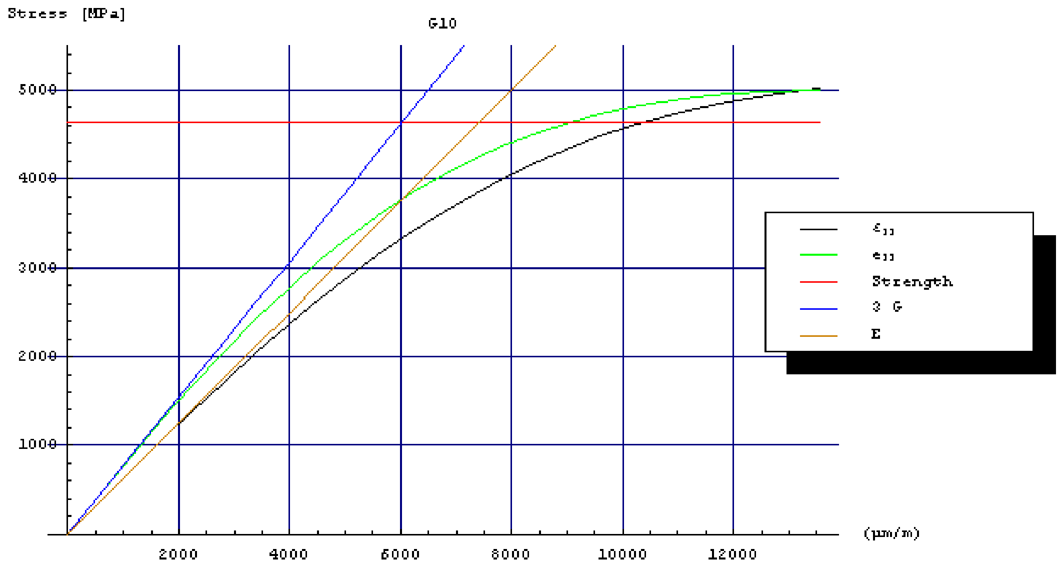
Stress [MPa]
G10
5000
4000
3000
2000
1000
2000
4000
6000
8000
10000
12000
(μm/m)
ε11
e11
Strength
3 G
E